# THE ROLE OF ADHESION AND ELASTIC MODULUS ON THE SENSITIVITY OF ENERGETIC MATERIALS TO VIBRATION AND IMPACT

by

**Jason Alexander Wickham**

**A Dissertation**

*Submitted to the Faculty of Purdue University*

*In Partial Fulfillment of the Requirements for the degree of*

**Doctor of Philosophy**


Davidson School of Chemical Engineering

West Lafayette, Indiana

May 2021

# THE PURDUE UNIVERSITY GRADUATE SCHOOL
# STATEMENT OF COMMITTEE APPROVAL

**Dr. Stephen Beaudoin, Co-Chair**
David School of Chemical Engineering

**Dr. Steven Son, Co-Chair**
School of Mechanical Engineering

**Dr. Jan-Anders Mansson**
David School of Chemical Engineering

**Dr. You-Yeon Won**
David School of Chemical Engineering

**Approved by:**
Dr. John A. Morgan

*To Caroline and Anthony*

# ACKNOWLEDGMENTS

This research was supported by the U.S. Air Force Office of Scientific Research (USAFOSR) under program manager Martin Schmidt through grant no. FA9550-15-1-0102. The content does not necessarily reflect the position or policy of the U.S. federal government, and no official endorsement should be inferred.

My eternal gratitude to Stephen Beaudoin for his guidance and support through graduate school and through all the sublimely joyful challenges outside of it.

Sincere gratitude to Steve Son for his guidance, support, and for inspiring me to take the leap to a lifetime working with energetic materials

Thank you to Jeff Rhoads for the guidance and help when I found myself stepping into several fields at once

A special thanks to Alex Reichanadter for being a good roommate, fantastic gym buddy, and an even greater friend

Thank you to my Arizona Aegis: Davis Burk, Andrew Herschfelt, Tyler Somers, Carter Gilton

Thank you to my Boise Boys: Davis Gilton, Ian Rice

Thank you to my ChemE Comrades near and far

Thank you to my DnD Dreams for providing much needed solace in this personal Barovia: Amanda Braun, Dakota Scott, Kyle Uhlenhake, Jonathan Crosmer

Thank you to all those I'm snubbing on accident because I'm forgetful

Love to my family Caroline, Anthony, Kevin, Patrick, Shally, Wickhams, and Carthys

# TABLE OF CONTENTS

LIST OF TABLES ..... 7
LIST OF FIGURES ..... 8
ABSTRACT ..... 10
1. INTRODUCTION ..... 11
1.1 Motivation ..... 11
1.2 Overview ..... 11
2. BACKGROUND ..... 13
2.1 Hot Spot Formation and High-Frequency Excitation ..... 13
2.2 Drop weight experiments ..... 18
2.3 Mixing ..... 21
2.4 Adhesion ..... 22
2.5 Infrared Spectroscopy ..... 24
2.6 Geopycnometry ..... 24
2.7 Optical Microscopy ..... 25
2.8 Sensitivity Testing ..... 27
3. THE ROLE OF ADHESION AND BINDER STIFFNESS IN THE IMPACT SENSITIVITY OF CAST COMPOSITE ENERGETIC MATERIALS ..... 34
3.1 Drop Weight Impact Experiment Samples ..... 34
3.2 Work of Adhesion and Elastic Modulus Measurement ..... 35
3.3 Drop Weight Impact Statistical Software ..... 36
3.4 Drop Weight Impact Testing ..... 36
3.5 Results ..... 38
3.6 Conclusions ..... 44
4. THE ROLE OF BINDER ADHESION AND STIFFNESS IN HOT SPOT FORMATION IN ULTRASONICALLY EXCITED COMPOSITE ENERGETIC MATERIALS ..... 45
4.1 Sample Fabrication ..... 45
4.2 Excitation and Measurement ..... 47
4.3 Work of Adhesion and Elastic Modulus Measurement ..... 48
4.4 Heat Generation Rate and Density Measurement ..... 48
4.5 Results ..... 49
4.6 Conclusion ..... 57

5. THE ROLE OF BINDER ADHESION AND STIFFNESS IN HOT SPOT FORMATION IN COMPOSITE ENERGETIC MATERIALS DUE TO STRONGLY COUPLED ULTRASONIC EXCITATION ..... 59
5.1 Sample Fabrication ..... 59
5.2 Excitation and Measurement ..... 61
5.3 Work of adhesion and elastic modulus measurement ..... 62
5.4 Results ..... 62
5.5 Conclusion ..... 67
6. FINAL CONCLUSIONS ..... 69
WORKS CITED ..... 71
APPENDIX A: SUPPLEMENTARY GUIDE TO SELECT METHODS ..... 77

# LIST OF TABLES

Table 3.1: Polymer matrix components by parts for impact experiments ..... 35
Table 4.1: Polymer matrix components by parts for the ultrasonic experiments ..... 47
Table 4.2: Work of adhesion, with standard errors, for each polymer material ..... 55
Table 4.3: Elastic modulus, with standard errors, for each polymer material ..... 55
Table 5.1: Polymer matrix components by parts for the ultrasonic experiments ..... 60

# LIST OF FIGURES

Figure 2.1: A drop of liquid on a solid surface ..... 23

Figure 2.2: Contact angle at the edge of the interface between the liquid drop and the solid substrate where the angle formed is due to a balance of interfacial surface energies ..... 23

Figure 2.3: HMX crystal heated to reaction and gas production creating a “blown-out” pocket. 25

Figure 2.4 HMX crystal heated to reaction creating a pocket around the crystal ..... 26

Figure 2.5: HMX crystal heated to reaction ..... 26

Figure 2.6: HMX crystal heated to reaction ..... 27

Figure 2.7: Example determination of the 50% drop height ..... 28

Figure 2.8: Evolution of the corresponding sigma of the 50% drop weight test ..... 29

Figure 2.9: HTPB BDO 50% drop height determination ..... 30

Figure 2.10: HTPB BDO sigma evolution ..... 30

Figure 2.11: Probability density functions of several drop weight tests for PBXs with different works of adhesion and elastic moduli ..... 31

Figure 2.12: Cumulative density functions of several drop weight tests for PBXs with different works of adhesion and elastic moduli ..... 33

Figure 3.1: Drop weight tower schematic ..... 37

Figure 3.2: BAM impact test sample holder. ..... 37

Figure 3.3: Probability density functions as a function of the drop energy input ..... 40

Figure 3.4: Cumulative probability of reaction as a function of drop energy input ..... 40

Figure 3.5: Drop energy as a function of modulus with error bars which represent the standard error of the 50% drop height. ..... 42

Figure 3.6: Drop energy as a function of work of adhesion with error bars which represent the standard error of the 50% drop height ..... 42

Figure 3.7: Elastic modulus and work of adhesion for selected materials ..... 43

Figure 4.1: Experimental apparatus used to apply ultrasonic energy to the composite materials and to monitor the resulting temperature change ..... 48

Figure 4.2: Heat generation rate at the HMX particle embedded in each polymer material (D = delaminated samples; U = undelaminated samples) ..... 50

Figure 4.3: Even heating pattern on top surface of undamaged sample ..... 51

Figure 4.4: Characteristic circular heating pattern on top surface of damaged sample ..... 52

Figure 4.5: Temperature trace of the top surface of an undamaged HTPB sample..... 53

Figure 4.6: Temperature trace of the top surface of an undamaged HTPB sample..... 53

Figure 4.7: Temperature trace of the top surface of a damaged sample..... 54

Figure 4.8: Elastic modulus and work of adhesion for selected materials..... 56

Figure 4.9: Average heat generation rate at the debonded HMX particle embedded in each polymer material. ..... 56

Figure 5.1: Increase of the maximum surface temperature of strongly coupled ultrasonic samples after 15 seconds..... 63

Figure 5.2: Average max surface temperature rise at the top surface of the polymer samples with standard deviations as error bars..... 64

Figure 5.3:Maximum surface temperature rise due to ultrasonic excitation of Sylgard 184/527. 65

Figure 5.4: Maximum surface temperature rise due to ultrasonic excitation of Sylgard 15:1..... 66

# ABSTRACT

The transformation of mechanical energy into thermal energy within composite energetic materials through various thermomechanical mechanisms is thought to lead to the creation of localized areas of intense heating. The growth of these "hot spots" is responsible for the bulk reaction or decomposition of the energetic material. Understanding the formation and growth of these hot spots has been an active area of research particularly for high-speed impact and shock conditions, but further work remains to be done in particular with respect to hot spot formation due to periodic mechanical excitation. Previous literature has established that many potential thermomechanical mechanisms may act at the interface between the constituent components of a composite energetic material. In order to provide further insight and guidance into the design of safer and more resilient energetic materials, the role of adhesion on hot spot formation for polymer bonded explosives (PBXs), a subset of composite energetic materials, was explored. Single HMX (1,3,5,7-tetranitro-1,3,5,7-tetrazocane) crystals in polymer blocks were subjected to ultrasonic excitation and subsequent heating was captured via infrared thermography. Subsequent testing of HMX PBXs using a drop weight tower captured changes in the sensitivity of the energetic material. Variation of the polymer binder allowed for a range of adhesive and mechanical properties to be examined. These experiments on the role of adhesion under these kinds of excitations provided insight into how mechanical energy is being transformed into localized heating.

# 1. INTRODUCTION

## 1.1 Motivation

The main objective of this work is to elucidate the role of adhesion in the transformation of incident mechanical energy into localized thermal energy within a composite energetic material such as a polymer bonded explosive (PBX). It has been demonstrated by previous literature that the formation of localized areas of intense heating or "hot spots" is often responsible for the initiation of the bulk energetic material. The transformation of mechanical energy into thermal energy is thought to occur through a number of mechanisms which are dependent on a number of factors such as the type of mechanical excitation and the composition of the energetic material. In particular, there are a number of these mechanisms which occur at the interfaces between a polymer binder and a crystalline energetic inclusion. Investigating the role of adhesion at this interface provides a way to understand and quantify the transformation of mechanical energy into thermal energy. A simplified approach using relatively low-energy sources of excitation such as ultrasonic vibration or drop weight impact allows for a more effective interrogation of this complex process. Utilizing a simplified system of a single crystal in a block of polymer, the ultrasonic experiments provide insight into how adhesion influences the periodic dissipation of mechanical energy at a single interface. While the mechanical insult in a drop weight test is markedly different from an ultrasonic test, previous literature has also suggested interfacial properties may be critical to understanding the impact sensitivity of an energetic material. For these tests, using samples with a high solids loading of energetic crystals and determining the sensitivity of the PBX allows for insight into the interaction between adhesion and hot spot formation. A thorough understanding of the role of adhesion in the sensitivity of energetic materials to various mechanical insults will allow for the design of much safer energetic materials while potentially opening new avenues for increased performance.

## 1.2 Overview

This work begins with a review of literature on hot spot formation along with a focus on research concerning vibration-induced hot spots and drop weight sensitivity testing in Chapter 2. Several of the methods for evaluating material properties are also discussed here along with the process

for selecting an appropriate measure of adhesion. A discussion of the statistical approach for the impact testing is also included. The drop weight experiments and results are discussed throughout Chapter 3. Various binders were utilized in order to vary the elastic modulus and work of adhesion between the energetic crystal and polymer binder. These materials were also utilized for ultrasonic testing with weakly-coupled samples as discussed in Chapter 4.

# 2. BACKGROUND

## 2.1 Hot Spot Formation and High-Frequency Excitation

Energetic materials can be generally considered to be materials which undergo rapid exothermic reactions liberating the large amount of chemical energy stored within their constituent molecular bonds. These materials can be broadly characterized based on application as explosives, propellants, or pyrotechnics. Many of these materials are susceptible to initiation or ignition by incident energies far below what would be required to raise the bulk of the material to decomposition temperature. It was commonly thought that this behavior was the result of the formation of localized areas of significantly higher temperatures than the bulk material. The formation of these hot spots was due to the transformation of the incident energy from mechanical, chemical, or other sources into thermal energy. This thermal energy was then responsible for the subsequent thermal decomposition of the energetic material leading to further generation of thermal energy [1-3]. If the reaction liberates sufficient energy, the hot spot will grow and potentially lead to the reaction of the bulk of the energetic material. The size, temperature, and duration of hot spots varies with excitation source and material, but the characteristic localization of energy leading to bulk decomposition remains the same [2, 3].

The mechanisms by which hot spot formation was suggested to occur can be varied and complex, but Field [1] suggested that they could ultimately be categorized into several distinct mechanisms such as adiabatic compression of trapped gasses, cavity collapse, friction between two surfaces, localized adiabatic shear, viscous heating of extruding material, heating at crack tips, and heating at dislocation pileups. For the purposes of this investigation. which seeks to understand the role adhesion plays in hot spot generation and sensitivity, several of these heating mechanisms are of particular interest. Given that adhesive forces occur at the interface between two materials, the frictional dissipation of energy at the interface was of particular interest. While other mechanisms may contribute to the formation of hot spots under ultrasonic excitation or impact, the frictional interaction provides a natural starting point to examine the role of adhesion in these systems. It should be noted in particular that other hot spot generation routes are still expected to contribute in these experiments, but the design should allow for frictional dissipation to be the dominant contributor.

While the sensitivity of composite energetic materials to mechanically-driven initiation has been an active area of research for many years, the focus has remained mainly on shock and non-shock impact excitation with the exception of some vibrational studies by Loginov [4-6] as well as Range, Miller, and Woods [7-10]. The demand for high-performance energetic materials has recently motivated the study of hot spot formation due to high-frequency vibration. The first renewed efforts to study hot spot formation in energetic materials due to high-frequency mechanical excitation have mainly focused on a frequency range from the tens to the thousands of kilohertz [8, 11-13]. Within this range where hot spot formation has been demonstrated, previous studies have suggested that the design of safer energetic materials requires that particle-binder interactions be better understood [8, 9]. Likewise, understanding the effect of the mechanical properties of binders on the thermomechanical response of particle-binder systems was also critical.

In order to isolate the influence of desired physical properties on PBX sensitivity, it was useful to reduce the complex mix of chemicals and particulates in the energetic material to a simplified system of a single energetic polycrystalline solid encased in polymer binder. Mares *et al*. utilized this approach with discrete energetic and inert inclusions encased in a polydimethylsiloxane (PDMS) binder (Sylgard 184) in order to examine the mechanisms responsible for the thermochemical response of energetic materials under ultrasonic excitation [8]. When the samples were excited with a piezoelectric transducer, heating at the surface could be observed via infrared thermography. The authors suggested that this was due to both viscoelastic dissipation and inclusion-binder interactions with heating observed for both energetic and inert inclusions. This was supported by a demonstration that variation of the excitation frequency could be used to cause either viscoelastic bulk heating or localized heating near the inclusion surface. Further evidence of these complementary and distinct modes of heating was found by comparing the heating observed at the top surface of the polymer block to the movement of the polymer surface as captured via a laser Doppler vibrometer. The authors highlighted the potential impact of these mechanisms by demonstrating that ammonium perchlorate (AP) and cyclotetramethylene-tetranitramine (HMX) could be driven to thermal decomposition upon application of sufficient ultrasonic energy at particular frequencies. By applying a model for a point heat source located at the depth of the single inclusion in a volume of binder, the heat generation rate and temperature at the surface of the inclusion were determined quantitatively. This yielded temperatures in excess of what would be required for thermal decomposition suggesting that modern composite energetic

materials could be vulnerable to ultrasonic excitation [14]. The evolution of the thermomechanical heating was further examined via synchrotron X-ray phase contrast imaging and diffraction. This demonstrated that the heating seems to occur in a three-step process where the sample heating was first dominated by viscoelastic dissipation. Delamination then occurs due to the thermal expansion of the material, allowing frictional dissipation to occur, culminating in the decomposition of the energetic material and the release of chemical energy [11].

Miller *et al.* continued investigations into this form of excitation with a study on the impact of crystal morphology on the thermomechanical response of an embedded AP crystal in Sylgard 184 [15]. It was observed that the degree of localized heating was not altered by crystal morphology. Rather, the probability of such heating was greater for irregular crystals compared to more spherical crystals. This provided strong evidence for the presence of two distinct mechanisms for transforming mechanical work into thermal energy. The first was viscoelastic dissipation of the energy as the polymer was stressed and relaxed leading to low-level heating of the bulk of the material. Modeling efforts using analytical stress and displacement solutions to describe a high-frequency compressional plane wave interacting with a rigid HMX sphere in Sylgard 184 demonstrated significant heating due to scattering of the compression waves [9]. The second mechanism was the result of frictional heating at the surface of the inclusion leading to strong localized heating. It was suggested this frictional dissipation was enabled by the delamination of the polymer from the surface of the crystal and that the delamination could be promoted by irregular surfaces. This conclusion was further supported by work performed by Roberts *et al.* that utilized high-speed microscopic imaging to observe ultrasonically excited single crystal samples encased in binder. It was observed that δ-HMX with a rough surface experienced a greater degree of heating as compared to smooth β-HMX, which did not show signs of delamination or heating sufficient to melt or decompose the crystal [12].

Pursuing a similar path of ultrasonic excitation, Chen *et al.* utilized an ultrasonic horn to more strongly excite a field of number of crystals of either cyclotrimethylene-trinitramine (RDX) in Sylgard 182 or sucrose encapsulated in hydroxyl-terminated polybutadiene (HTPB) [13]. At these high excitation energies, mid-wave infrared (MWIR) thermography inferred localized temperatures in excess of 500 K within 150 ms with preferential heating occurring at or near the crystal-binder interface. The authors suggested these results provided evidence of two possible heating mechanisms: a localized viscoelastic dissipation mechanism enhanced by wave scattering

due to the interface between materials of differing impedance, and a frictional dissipation mechanism wherein the kinetic energy was dissipated as frictional heating due to disparate motion of the polymer and crystal materials. To investigate the frictional dissipation mechanism, You *et al.* [16] performed similar experiments with crystals coated in either polytetrafluoroethylene (PTFE) or liquid polyethylene glycol (PEG) and cured in Sylgard 182. This coating isolated the crystal from the polymer during the curing process, preventing the intimate molecular contact necessary for strong interfacial adhesive forces from developing. This allowed preferential generation of intense hot spots on the coated crystals when subjected to ultrasonic excitation, providing evidence in favor of the frictional heating mechanism. Examination of the excited particles after the conclusion of the experiment using a scanning electron microscope revealed smoothed and worn crystal surfaces which the authors suggested provided evidence of frictional damage.

In work by Men et al., an ultrasonic horn was once again utilized in order to gather data on the thermal explosions resulting from excitation of an embedded and lubricated energetic crystal. An IR camera and linear array detector were used in order to gather spatial and temporal information during the early stages of excitation. A two-stage thermal explosion was observed for RDX and HMX with the authors suggesting the first was a solid-state explosion which was quenched by the formation of a gas pocket, and then the second gas-phase explosion resulted from adiabatic heating of the gases in the gas pocket or from a delayed reaction due to relatively slower chemical kinetics. The authors suggest that the investigation of this two-stage process demonstrated a need to further examine how the relationship between ultrasonic excitation and hot spot formation changes as the energetic material heats, melts, and reacts [17].

While single crystals provided some insights into real PBX behavior, Roberts *et al.* investigated the effects of crystal-crystal contact utilizing a simplified system of three HMX crystals embedded in Sylgard 184 binder [18]. Two different geometries were utilized for the crystal configurations. The first configuration constrained the crystals to be separated by less than 400 μm without contacting each other, and the second placed the crystals such that at least two points of contact were observed between them. It was determined that the heating due to ultrasonic excitation for the ‘in contact’ configuration was much greater than the heating observed in the ‘separated’ configuration. It was suggested that this was due to frictional dissipation at the points of contact or frictional dissipation enabled by delamination of the binder near the points of contact.

Further experimentation was performed by purposely delaminating the binder from the crystal through the use of mechanical force on the cured samples of both configurations and subjecting the delaminated samples to ultrasonic excitation. For the 'separated' samples, significantly greater heating was observed for the delaminated samples than for the undamaged samples. While crystal-crystal contact and delaminated crystal initial conditions generally led to a similar degree of heating, analysis of the results showed that the delamination was a stronger predictor of increased heating for both 'in-contact' and separated samples. This also provided evidence that delamination introduced modes of heating, such as frictional dissipation, which could far exceed the heating due to viscoelastic effects for this particular system and excitation conditions.

The importance of the stiffness and adhesive properties in the failure of composites such as energetic materials was explored via ellipsometry and nanoindentation techniques in work by Yeager *et al*. [19]. Recrystallized HMX was coated in either estane (a thermoplastic polyurethane) or estane with nitroplasticizer via a dip coating procedure before being characterized and subjected to nanoindentation. It was observed that a weaker interface could be formed with the addition of plasticizer leading to prompt delamination of the binder material from the crystal when relatively low stresses were applied. It was posited that this behavior could be responsible for the safety characteristics of the PBX 9501 formulation, but the authors cautioned that this method of improving safety characteristics could lead to sensitization of the mixture to other insults once damage has taken place. Due consideration must be paid to how sensitivity may evolve or how decreasing the sensitivity to a particular insult may result in increased sensitivity to another. This was exemplified in how curing times, the viscosity of the uncured base, and the health hazards associated with HTPB-based polymers have encouraged the consideration of Sylgard in some research settings as an alternative binder for PBXs. In work by Elbeih *et al.*, the utility of Sylgard as a desensitizing binder was examined and demonstrated via large decreases in the drop weight and friction sensitivities compared to the pure explosive crystal components [20]. Sylgard-based PBXs were also shown to have lower sensitivities than selected commercial PBXs for impact and friction [21]. It was evident that the material properties of PBX binders play a considerable role in the sensitivity of a compounded explosive.

## 2.2 Drop weight experiments

The drop weight impactor experiment has a long history in the study of the sensitivity to impact of energetic materials [2, 22, 23]. In drop weight impactor studies, a sample was placed on an anvil and subjected to impact via the gravitationally-driven fall of a striker of known mass from a chosen height. The experimental results are categorized as go or no-go based on whether or not ignition or initiation of the energetic material results from the impact. Repeated testing allows for statistical characterization, including the determination of a drop height at which a sample has a 50% probability of reacting (on a particular apparatus). For a given height an initiation energy can be calculated,

$$E_{impact} = mgh \tag{2.1}$$

which is the equation for gravitational potential energy. Here, $E_{impact}$ was the energy of the impact, $m$ was the mass of the striker, $g$ was the acceleration due to gravity, and h was the chosen height of the drop weight at the onset of the experiment. The 50% drop height or energy was reported traditionally, but statistical distributions can also be calculated. It was important to note that the impact energy was a measure of the total energy imparted to the sample and anvil rather than strictly the amount of energy required to ignite the material, which partially accounts for the probabilistic nature of the experiments [24, 25]. While the setup and execution of this type of experiment appears to be quite simple, the drop weight test can suffer from poor repeatability and often the results are only used to crudely rank sensitivities of energetic materials [2, 25]. Nevertheless, the drop weight impact test remains one of the most commonly used methods for characterizing the response of energetic materials to low speed impacts. It has been utilized to great effect in studying the role of chemical composition on impact sensitivity with authors demonstrating consistent links between particular chemical configurations and sensitivity [26-28]. Modeling work has also made use of the impact test results in order to correlate various solid-state criteria to impact sensitivity [29-31]. Consequently, drop weight impact testing remains a valuable tool for evaluating changes in sensitivity.

One of the most significant ways that the drop weight impact test has been improved was through the use of optically clear anvils and impactors. While this does not inherently solve any of the consistency issues experienced with drop weight impact testing, these modifications allow for the introduction of high-speed photography and reveal several important dynamic phenomena. Primarily, they allow for observation of how material failure is related to the sensitivity of

energetic materials and demonstrate that a countable number of hot-spots can be responsible for bulk decomposition for a low speed impact scenario [25, 32]. Combined with earlier works where it was demonstrated that the bulk heating of the material was insufficient to raise its temperature appreciably [2], the observation that localized heating (or "hot spots") was responsible for reaction of a sample suggests that interfacial surface chemistry could influence the ultimate sensitivity of an energetic material [1].

While most drop weight impact experiments are carried out for pure energetic materials in the form of loose powders, an exploration into PBXs containing thermoplastic polymers was performed in work by Swallowe and Field [33]. In a series of drop weight experiments performed on equipment designed for high speed photography, cylinders of thermoplastic polymers and pressed pellets of cyclotetramethylene tetranitramine (HMX) were subjected to impact. In these experiments, it was observed that polymers which could desensitize a mixture generally had a high latent heat of fusion as well as a tendency to deform plastically without catastrophically failing. Polymers that failed catastrophically were seen to sensitize the mixture. These polymers created regions where polymer and energetic powder would rapidly flow through or around each other, generating regions of intense thermal dissipation/heating due to friction. This in turn produced many hot-spots and ignition of the energetic material. Split-Hopkinson bar experiments with energetic materials resulted in significant observed shear banding that indicated particle-particle interactions were critical for thermal decomposition within the PBX samples. Importantly, this shear banding was a function of particle spacing (or loading) and binder stiffness[34]. Ultimately, this series of experiments demonstrated that the manner in which the polymer material fails, or deforms, can affect the sensitivity of the material and that determination of an explicit or empirical relationship between physical and chemical properties of the binder and sensitivity may be plausible.

Schedlbauer and Kretschmer[35] varied binder properties and particle size in order to obtain PBXs with similar elastic moduli while containing differently sized particles. They evaluated sensitivity using standard drop weight impact tests, in addition to friction, shock (via large-scale gap tests), and bullet impact studies. The results demonstrated that for a given elastic modulus of the composite material, sensitivity can be decreased by utilizing finer energetic particles. The authors attributed these results to defects within the crystals or changes in porosity

of the charges, but the role of the mechanical properties in the impact sensitivity of the composite remained unclear.

Mechanical properties were explored by Manner and Yeager[36] in a study examining the role of the mechanical properties on the deformation and failure of PBXs. By compressing then taking CT images of the PBX samples, the authors demonstrate that both the mechanical and adhesive properties contribute to stark differences in how the PBX fails. The softer sample tended to flow under compression versus the cracking and separation observed in the stiffer sample. Similarly, testing a series of PBX samples with stronger adhesion demonstrated a shift in the failure mode from intergranular to mixed inter- and transgranular failure. These experiments demonstrated the profound influence that binder properties can have on PBX failure, and suggest that it may be possible for these properties to have an influence on other behaviors such as sensitivity.

Martin and Yee[37] performed two studies to relate the composite mechanical, interfacial surface properties, and sensitivities of PBXs. The first study mixed various commonly used binders with the explosive crystal cyclotrimethylenetrinitramine (RDX). The outcome of this study determined the values of the surface energies and various mechanical properties that would be of interest for investigating their role in sensitivity. This work paved the way for a second study on various mechanical properties, including dewetting, and sensitivity. By assuming that the adhesive bond between crystal and binder was the weakest bond in the energetic composite materials, the critical radius of detachment of a spherical inclusion in elastic material could be related to the energy absorbed in debonding, the stress, the elastic modulus, and the Poisson's ratio[38]. It was assumed that dewetting was associated with the breaking of the adhesive bond between the crystals and the binder and was functionally the same as delamination wherein it describes the peeling away of one surface from another. The relationship used to estimate the critical arrangement for detachment was

$$EW = Kr^{*}\sigma^{2} \tag{2.2}$$

where $E$ was the elastic modulus of the composite, $K$ was a constant which was a function of Poisson's ratio, $r^*$ was the critical inclusion radius, $W$ was the energy absorbed in debonding or work of adhesion, and $\sigma$ was the stress at the onset of dewetting which was taken to occur at a volume dilation of 1% under tensile stress [39]. For systems with constant particle size, constant $r^*$, Eq 2 suggests that a plot of $\sigma^2$ as a function of $E$ should be linear with a constant slope

proportional to *W*, which was confirmed experimentally for an energetic material composed of hydroxyl-terminated polybutadiene (HTPB) and RDX[39]. While the authors also evaluated the sensitivities of the mixtures to drop weight impact, they did not systematically vary the mechanical and adhesive properties of the binder to explicitly investigate the relationship of these properties to impact sensitivity. It was noted that surviving damaged samples were more sensitive and that a slight reduction in sensitivity was observed for damaged samples that were allowed to rest for significant amounts of time.

Based on these previous studies, a link may exist between the impact sensitivity of an energetic composition and both the mechanical and particle-binder interfacial properties of the composition. This current work explicitly explores this relationship by systematically varying the elastic modulus and work of adhesion in a homologous family of PBX energetics, to help guide the development of new PBX systems.

## 2.3 Mixing

Given that a range of material properties was necessary in order to explore the role of adhesion in hotspot formation and sensitivity, Sylgard and HTPB were chosen as binder systems. The variation of the Sylgard polymers was accomplished by varying the amount of curative added to the base and substituting a significant fraction of Sylgard 184 with Sylgard 527, a softer PDMS polymer blend. Based on available literature, this method allowed for an order of magnitude variation in the modulus of the cured polymer compound without significantly altering its surface energy [40].

The variation of the properties of the HTPB polymers was accomplished through the introduction of butane diol as a chain extender which allowed for a threefold increase in the modulus without significant changes to the surface energy of the final compound. The mixing ratios for HTPB were determined using the following equation [41, 42]:

$$\frac{W_{curative}}{EW_{curative}} = (IR)\left(\frac{W_{HTPB\ compound}}{EW_{HTPB\ compound}} + \frac{W_{Bonding\ agent}}{EW_{Bonding\ agent}}\right) \tag{2.3}$$

In **Equation 2.1**, *W* is mass, IR is the index ratio or the ratio of NCO to OH, and *EW* is equivalent weight. Equivalent weight is the effective grams per reactive group which can also be stated as the ratio of the molecular weight of the component to the number of reactive groups per molecule.

While no bonding agent was utilized, the mass and equivalent weights of butane diol simply substituted into the same place in the equation.

## 2.4 Adhesion

Quantifying the adhesion between energetic inclusions and polymer binders is a difficult task that has been approached by some authors through measuring the pull-off force or some equivalent metric [38, 43-45]. While this incorporates elastic and inelastic contributions, these methods make it difficult to accurately assess the influence of a single property across different composite mixtures. Consequently, it is important to utilize a more fundamental measure of adhesion that can be varied relatively independently from mechanical properties. The adhesion at the interface between the energetic inclusion and the polymer binder can be characterized using the thermodynamic work of adhesion which describes the increase in free energy from creating two surfaces. This approach accounts for the fundamental intermolecular forces responsible for adhesion and provides a route for discriminating between weak and strong adhesion. The thermodynamic work of adhesion can be calculated from the surface energies of each component in a system of contacting materials. These surface energies can be determined from simple contact angle experiments as the angle formed between the liquid, solid, and vapor phases was empirically indicative of the involved intermolecular forces. In work by Yeager *et al.* a contact angle measurement method was used to evaluate the adhesive properties of a number of fluoropolymers with potential applications as explosive binders [46]. The general process was outlined below including important equations.

First, the work of adhesion can be written as below where the subscripts on each interfacial surface energy represent a solid-vapor, liquid-vapor, or solid-liquid interaction [47].

$$W_a = \gamma_{SV} + \gamma_{LV} - \gamma_{SL} \tag{2.4}$$

An explicit relationship between the angle formed and the interfacial surface energy components can be found in Young's equation for the equilibrium of a droplet [48].

$$\gamma_{LV} \cos\theta = \gamma_{SV} - \gamma_{SL} \tag{2.5}$$

In order to avoid underestimating the true surface energy, the surface energies must be split into polar and dispersive components which are denoted with the superscripts *p* and *d* respectively [49].

$$\gamma_{SL} = \gamma_{SL}^{p} + \gamma_{SL}^{d} \tag{2.6}$$

Further, the interfacial surface energy can be represented as a geometric mean of the interacting surface energies [50].

$$\gamma_{12} = \gamma_1 + \gamma_2 - 2\sqrt{\gamma_1{}^d\gamma_2{}^d} - 2\sqrt{\gamma_1{}^p\gamma_2{}^p} \tag{2.7}$$

This can be substituted into a final modified Young's equation given below [50].

$$\left(\frac{\cos(\theta)+1}{2}\right)\left(\frac{\gamma_{lv}}{\sqrt{\gamma_l{}^d}}\right) = \sqrt{\gamma_s{}^p}\left(\frac{\sqrt{\gamma_l{}^p}}{\sqrt{\gamma_l{}^d}}\right) + \sqrt{\gamma_s{}^d} \tag{2.8}$$

Polar and dispersive components of the liquids can be obtained from literature, allowing for determination of the polar and dispersive components of an unknown solid via a simple linear regression [50-52]. An example of this process is shown in **Figure 2.1** and **Figure 2.2** where a drop of a liquid is placed upon a surface and the angle measured is a product of the various surface energy interactions at the interface.

Figure 2.1: A drop of liquid on a solid surface

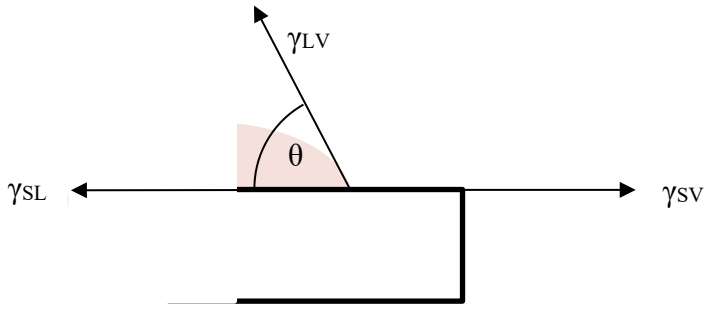


Figure 2.2: Contact angle at the edge of the interface between the liquid drop and the solid substrate where the angle formed is due to a balance of interfacial surface energies

The importance of the stiffness and adhesive properties in the failure of composites such as energetic materials was explored via ellipsometry and nanoindentation techniques in work by Yeager *et al*. [19]. Recrystallized HMX was coated in Estane® or Estane® with nitroplasticizer via a dip coating procedure before being characterized and subjected to nanoindentation [19]. It was observed that a weaker interface could be formed with the addition of plasticizer leading to prompt delamination of the binder material from the crystal due to relatively low stresses. It was

posited that this behavior could be responsible for the safety characteristics of the PBX 9501 formulation, but the authors cautioned that this method of improving safety characteristics could lead to sensitization of the mixture to other insults once damage has been applied. Consequently, due consideration must be paid to how sensitivity may evolve or how decreasing the sensitivity to a particular insult may result in sensitization to another. Both the adhesive and mechanical properties of the constituents in a PBX contribute to the specific sensitivities of the overall PBX.

## 2.5 Infrared Spectroscopy

In order to evaluate the role that adhesion plays in the transformation of mechanical energy to thermal energy at the interface, it is necessary to capture the heating rate. In previous works this has been accomplished with the use of infrared (IR) thermography. IR thermography is particularly suited for examination of hot spot formation, but there are obvious challenges to overcome due to the short duration and violent nature of energetic material decomposition. However, using a simplified PBX sample containing discrete, countable energetic inclusions in a block of polymer has proven to be an effective method for previous authors [12, 18, 53]. These methods have leveraged the longer timescales available during ultrasonic excitation in order to glean insight about specific thermomechanical mechanisms.

## 2.6 Geopycnometry

For the purposes of calculating heat generation rates as utilized in this study, the density of the polymer material must be determined. In order to address this, geopycnometry was employed. Geopycnometry is a technique for measuring the volume of an unknown solid by measuring the displacement of a freely flowing dry powder medium. The powder particles are sufficiently small to allow for close packing around the sample. The testing apparatus consists of a precisely machined glass cylinder and an electrically controlled piston. A baseline volume is first established by charging the cylinder with an initial volume of the dry powder. The cylinder and piston are vibrated as the piston compresses the volume of dry powder to a predetermined force limit in order to yield an initial volume. The mass of the sample is measured and then inserted into the opened cylinder with the initial mass of dry powder. The cylinder and piston are again vibrated and compressed to the same predetermined force limit. The sample density is then simply the sample

mass divided by the change in volume. The change in volume is a simple calculation as the cross-sectional area of the cylinder remains constant while the length is variable.

## 2.7 Optical Microscopy

Optical microscopy has been employed before in order to study some of the effects of ultrasonic excitation of energetic material. In particular, Roberts et al. used optical microscopy to investigate the various thermomechanical mechanisms responsible for transforming ultrasonic energy into thermal energy [12, 18, 53]. Optical microscopy proved essential for capturing phase changes in HMX crystals as well as the influence of crystal proximity on ultrasonic heating. While IR thermography is more than sufficient for capturing and comparing heating results, optical microscopy was necessary for measuring embedded crystal diameters and depths. This tool also proved useful for comparing to the previous literature and gave some insight into crystal shape.

**Figure 2.3** and **Figure 2.4** show an example HMX crystal embedded in a Sylgard blend and subjected to ultrasonic excitation. Over the course of a few seconds, sufficient thermal energy has been generated to cause significant gas production. The crystal heats, melts, produces gas, and eventually is quenched when the gas creates a sufficiently large pocket around the original inclusion or the gas escapes the original location and "blows-out" into the surrounding material. This is consistent with previous literature on ultrasonic excitation of energetic materials [12].

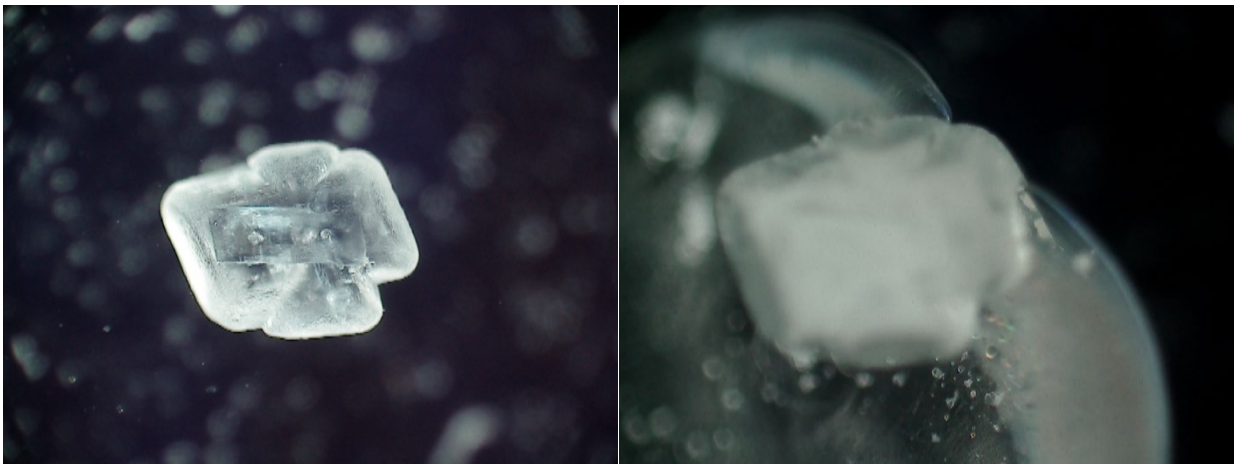

Figure 2.3: HMX crystal heated to reaction and gas production creating a "blown-out" pocket

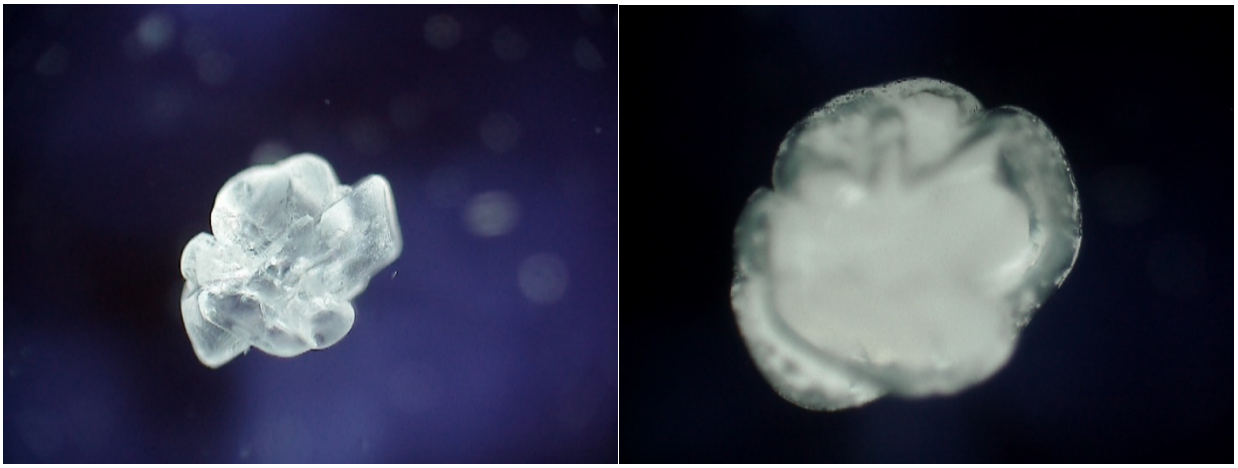

Figure 2.4 HMX crystal heated to reaction creating a pocket around the crystal

Optical microscopy was also useful for examining the morphology of the crystals as seen in **Figure 2.5** and **Figure 2.6**. In all of these images, the shapes of the crystals are highly irregular, having been drawn from production grade crystals. These production grade crystals are similar to the ones utilized in this study and so these videos provide insight into measured heating results.

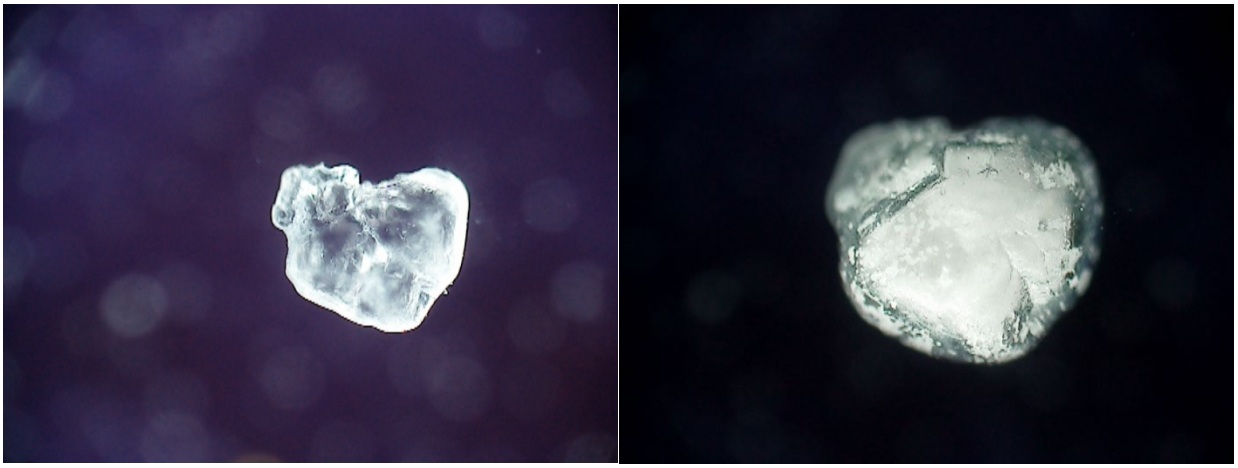

Figure 2.5: HMX crystal heated to reaction

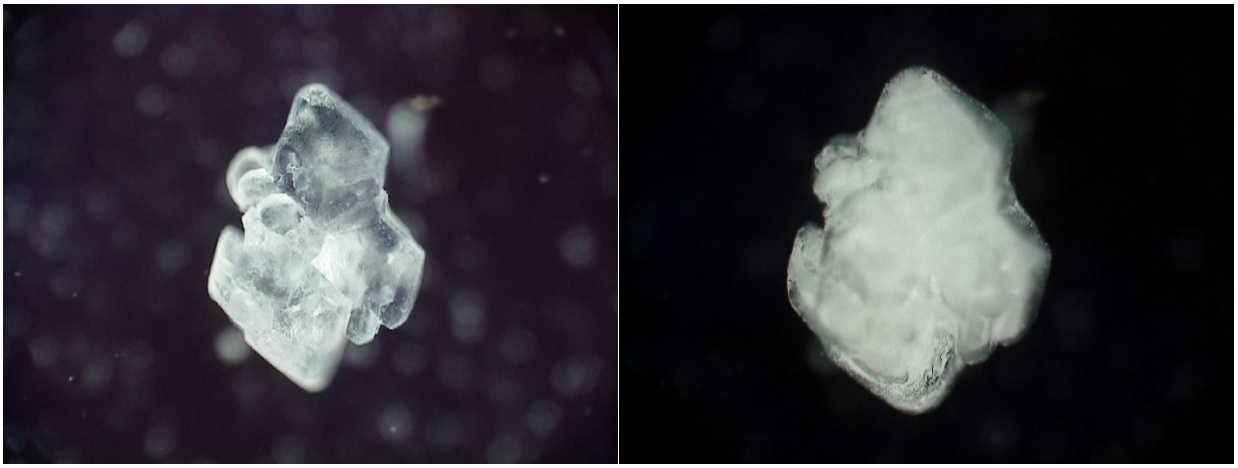

Figure 2.6: HMX crystal heated to reaction

## 2.8 Sensitivity Testing

A challenge associated with determining the sensitivity of a PBX material is that samples are consumed in the process of testing, if the testing drives the sample to decomposition or to a change in state.Evenin cases where there is no reaction or initiation, the necessary design of the test will damage the sample. Thus, it is not possible to directly measure the sensitivity parameters of interest. However, a number of statistical tests have been developed which seek to effectively and efficiently determine an estimated 50% drop height for detonation and the associated shape of the probability curve [54, 55]. The method chosen for this study utilizes the Neyer test in order to quickly determine the drop height parameters of interest. This test utilizes a D-optimal test which optimizes knowledge of the parameters of the curve while remaining fairly robust even when initial estimates of the mean and standard deviation are unknown. Effectively, this test provides the tester with the next testing level at which the most knowledge about the probability curve can be gained [56].

An example of this process can be outlined using a series of tests with a PBX consisting of 85 wt% HMX and 15 wt% Sylgard blend. The current predicted drop height and associated sigma (standard deviation) are tracked in **Figure 2.7** and **Figure 2.8** respectively. In this case, an initial predicted guess height of 76 cm was provided and testing began at 76 cm. The filled circle represents the current estimated 50% probability of reaction (PoR) height or the height at which 50% of samples can be expected to react. The *x* marks a ‘go’ case at the tested height (detonation occurred) and an empty circle represents a ‘no-go’ case at the tested height (no detonation

occurred). For example, the predicted 50% PoR height for trial 4 was 70 cm and the tested drop weight height was 86 cm which resulted in a go case. Thus, the predicted 50% PoR height decreased to 67 cm and the next test was conducted at 70 cm which resulted in a go case. Only when there is an "unexpected" result where a sample reacts when it is below the 50% PoR height does the Neyer Sentest provide useful statistical data beyond suggesting the next drop height. This occurs on trial 15 for this case and this "unexpected" result allows for the probability curve to be constructed.

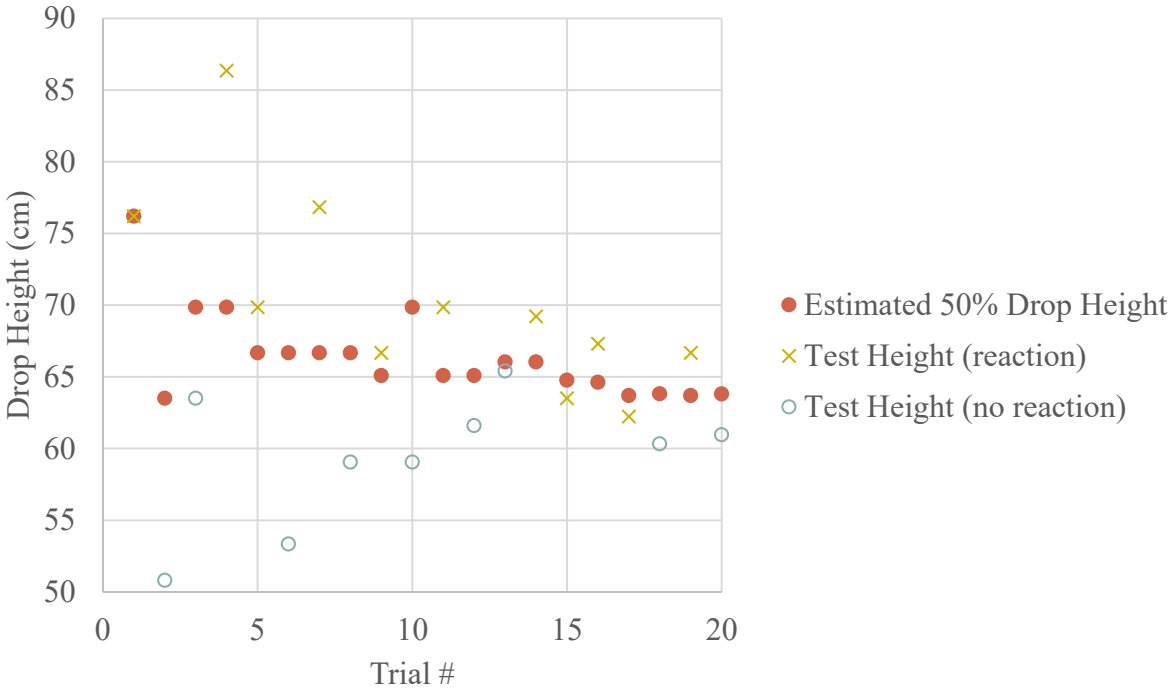


Figure 2.7: Example determination of the 50% drop height

It is useful at this point to examine the evolution of the sigma on **Figure 2.8** and note how until trial 15, the probability curves cannot be meaningfully constructed. Following the data from there, trial 16 returns an expected result and so the standard deviation decreases effectively sharpening the predicted probability curve. If this reflected the true standard deviation for this PBX, this would indicate that there was a sharp transition from no reaction to a reaction. This can be a good indicator of uniformity between samples and likely indicates that the true standard deviation is being calculated. Trial 17 yields an "unexpected" go-case and so the predicted sigma increases. The process of determining drop height is, by necessity, a stochastic process so a gradual

determination of each drop height parameter is to be expected. This can be seen earlier in **Figure 2.7** where the "unexpected" results do not significantly alter the predicted PoR height.

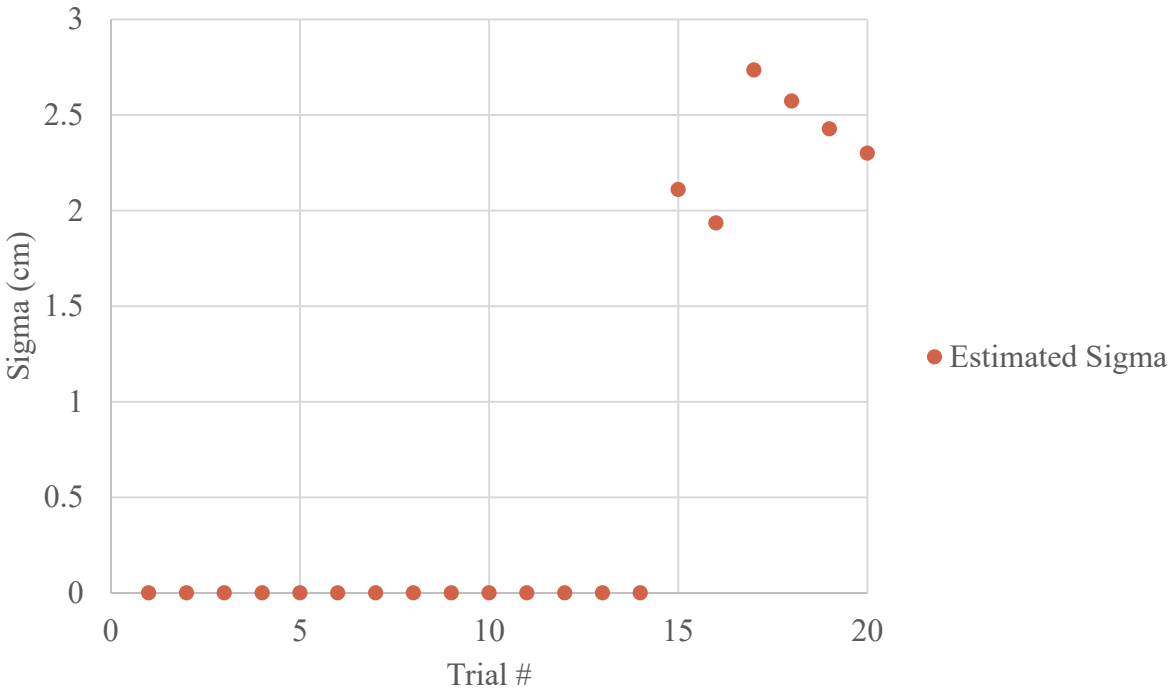


Figure 2.8: Evolution of the corresponding sigma of the 50% drop weight test

As there is no upper limit to how many tests may be performed, it is up to the experimenter to determine how many tests is sufficient to determine the PoR height and associated sigma. In this work it was determined that testing was completed when 10 successive trials were completed with "expected" results which was reflected in a consistently decreasing sigma value. This can be seen in **Figure 2.9** and **Figure 2.10** which were performed with PBXs containing hydroxyl-terminated polybutadiene (HTPB) with butane-diol (BDO) chain extenders. As before, no true probability curve can be constructed until trial 14. While the variation in the PoR height is relatively small compared to the magnitude of the drop height, the variation in the sigma demonstrates the gradual approach to a true estimate. As established before, testing was determined to be complete upon ten successive decreases in sigma. Of interest is that the impact of each "unexpected" result can be seen in both the higher sigma value and the more gradual decrease after each "expected" result. Consequently, greater confidence can be taken in the final reported sigma and PoR height value.

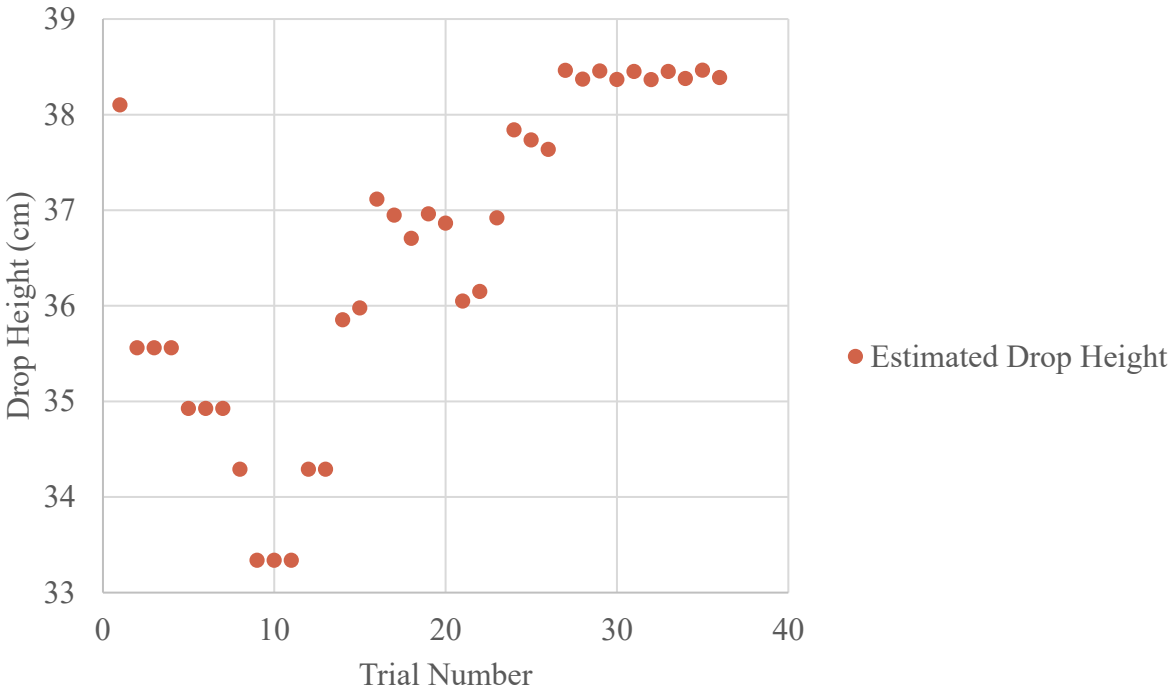


Figure 2.9: HTPB BDO 50% drop height determination

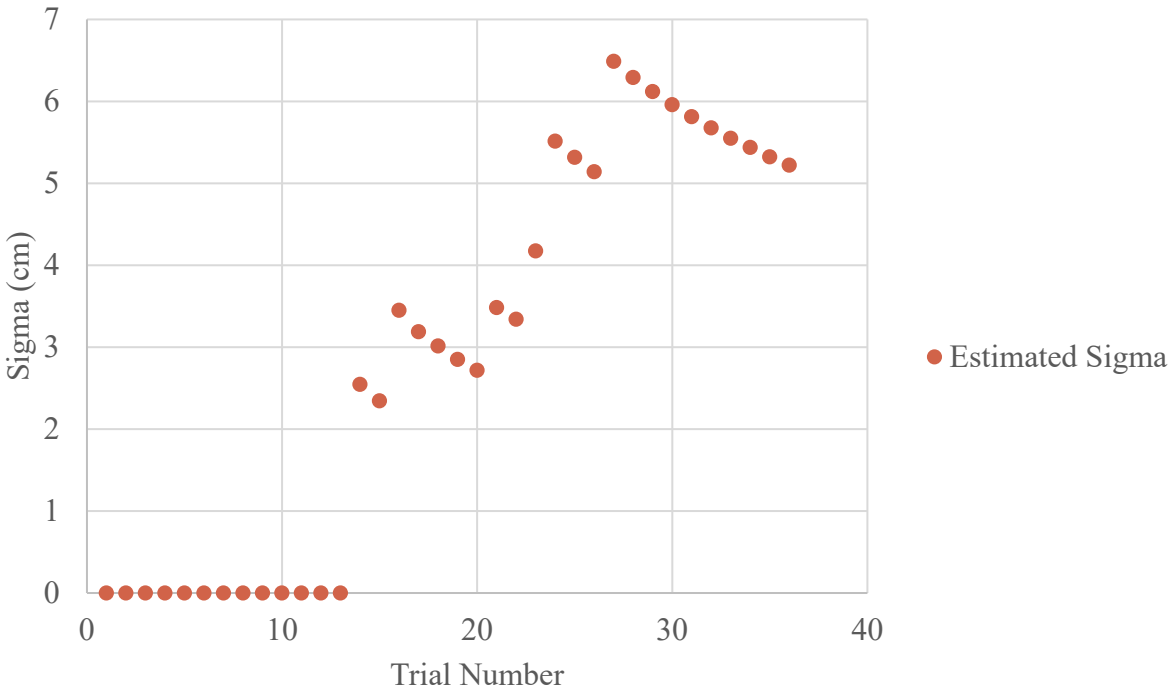


Figure 2.10: HTPB BDO sigma evolution

After the 50% PoR height and corresponding sigma have been determined for a chosen PBX material, the probability density function (PDF) and cumulative distribution function (CDF) that describe the impact sensitivity of the PBX can be constructed. As it has been assumed that the drop height of the PBX can be described using a Gaussian distribution, **Equation 2.9** can be employed.

$$PDF(x) = \frac{1}{\sigma\sqrt{2\pi}} e^{\frac{-(x-\mu)^2}{2\sigma^2}} \tag{2.9}$$

In **Equation 2.9**, $\sigma$ is the scale parameter and $\mu$ is the location parameter. For the purposes of this study with respect to impact testing, $\sigma$ is the estimated standard deviation and $\mu$ is the estimated 50% PoR height. Applying this and graphing the results yields PoR curves as pictured in **Figure 2.11**. In this figure, several PBXs with different polymers are utilized. These values represent the relative likelihood that a random sample of the PBX would yield a particular drop height.

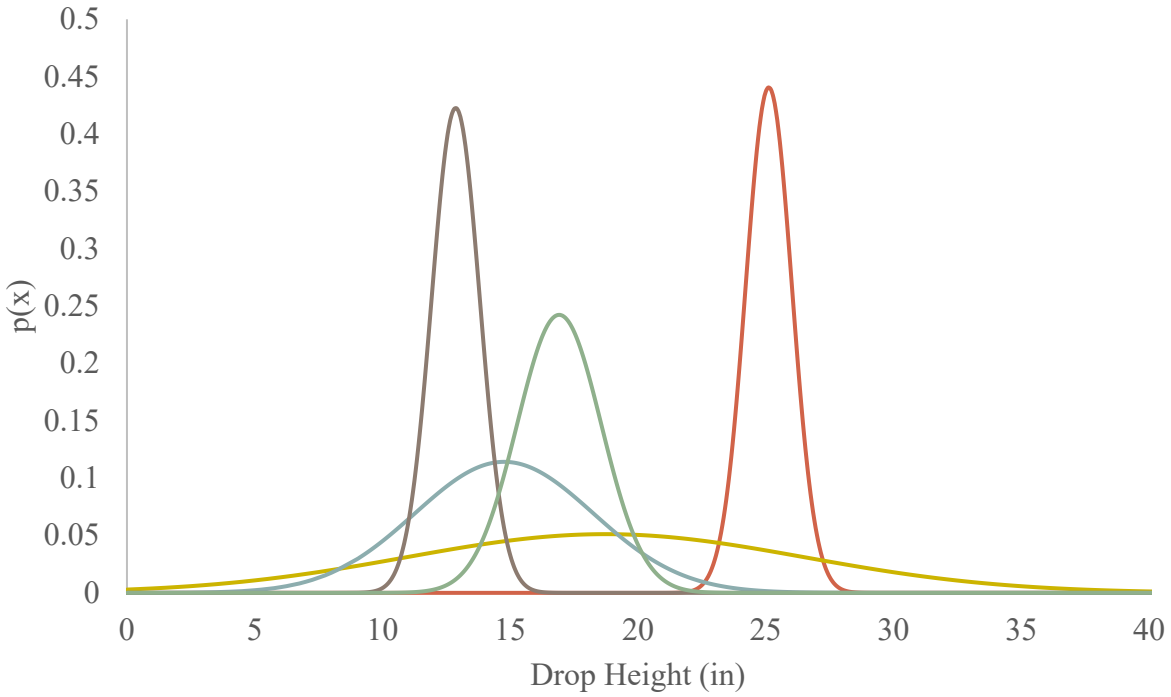


Figure 2.11: Probability density functions of several drop weight tests for PBXs with different works of adhesion and elastic moduli

By integrating **Equation 2.9**, **Equation 2.10** can be yielded which describes the cumulative distribution function $CDF(x)$. In this case, *erf* represents the error function. This form is more useful for comparing and understanding the results of the drop weight test.

$$CDF(x) = \frac{1}{2}\left[1 + erf\left(\frac{x-\mu}{\sigma\sqrt{2}}\right)\right] \tag{2.10}$$

Applying this to the previous data set, the results can be graphed as in **Figure 2.12**. The 50% PoR height is immediately apparent in this new presentation and can be easily compared by following the 0.5 line from left to right. These values are normally what is compared when 50% drop or PoR heights are reported within the literature. However, as most literature attempts to only compare drop heights for the purposes of crude sensitivity rankings, the spreads and their meaning are not often reported. Using the additional data from the generated cumulative density function curves, the effect of a larger or smaller deviation can be seen in the more gradual transition from "no-go" to "go" cases. For example, the yellow curve represents a sample that has a sharply defined 50% PoR where this transition occurs rapidly. The orange curve represents samples which have much higher 50% PoR heights, but the broader curve indicates significant variability with the PoR of the orange and yellow curves intersecting at about 12 in. Below this height, the samples represented by the yellow curves are predicted to quickly drop to practically 0% PoR. In contrast, the samples represented by the orange curves are predicted to have a not-insignificant PoR even below 10 in. Thus, samples which appear to superficially be more insensitive to drop weight impact (high 50% PoR) compared to "sensitive samples" (low 50% PoR), may represent a significant safety hazard at energies far below the 50% PoR.

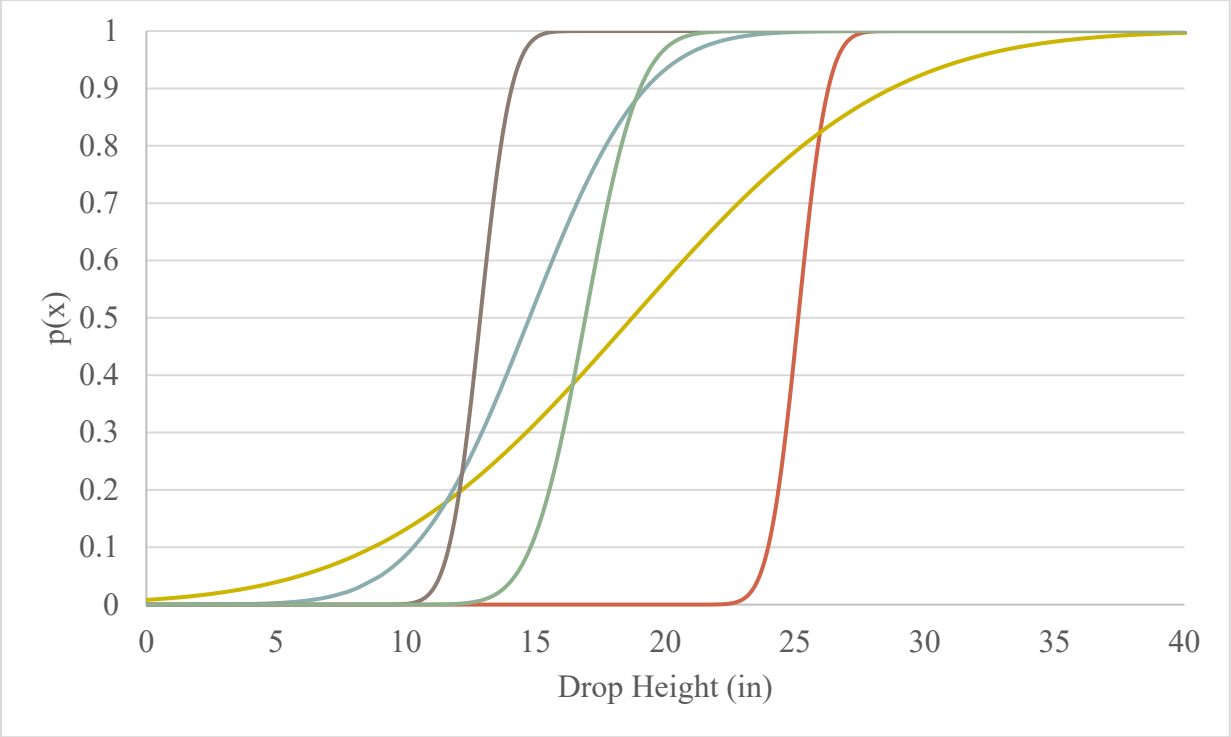


Figure 2.12: Cumulative density functions of several drop weight tests for PBXs with different works of adhesion and elastic moduli

While this provides some interesting insights, caution must be urged before making conclusive claims on sensitivity. Significant testing at low drop heights would be required to prove or disprove assertions of actual sensitivity at such heights. Ultimately, this kind of observation may be more helpful for identifying variability or sensitization due to damage in samples. It may also be of significant use for quantifying the roles of various failure mechanisms or the influence of various additives. In the course of this study, it was used to evaluate the influence of adhesion, but it has become clear that it could have significant value to future studies as well.

# 3. THE ROLE OF ADHESION AND BINDER STIFFNESS IN THE IMPACT SENSITIVITY OF CAST COMPOSITE ENERGETIC MATERIALS

The drop weight impactor experiment has a long history in the study of the sensitivity to impact of energetic materials [2, 22, 23]. There have been numerous studies which attempt to quantify the relationship between physical or chemical parameters and sensitivity, but the influence of adhesion remains an open question. Often most of the parameters of interest were completely mechanical, but based on these previous studies, a link may exist between the impact sensitivity of an energetic composition and both the mechanical and particle-binder interfacial properties of the composition [36, 37, 39]. This current work explicitly explores the relationship between adhesion and impact sensitivity by systematically varying the elastic modulus and work of adhesion in a homologous family of PBX energetics, to help guide the development of new PBX systems.

The objective of this chapter is to explore the relationship between adhesion and the sensitivity of PBXs to drop weight impact. This was accomplished utilizing HMX-based PBXs and swapping the polymer component between several different blends in order to obtain different works of adhesion and elastic moduli. By systematically determining both the predicted 50% probability of reaction drop height and the associated spread, conclusions about the influence of adhesion on these PBXs could be drawn. In particular, this work allowed for exploration of possible mechanisms responsible for the sensitivity behavior of PBXs. Portions of this chapter are reproduced from "The Role of Adhesion and Binder Stiffness in the Impact Sensitivity of Cast Composite Energetic Materials" in the Journal of Applied Physics volume 128, issue 21, paper 214902, 2020 [57] with the permission of AIP Publishing.

## 3.1 Drop Weight Impact Experiment Samples

Each drop weight impact sample consisted of a polymer binder and 85% HMX by weight. By utilizing HMX as the energetic component for all samples, significant variations in drop energy due to chemical composition were controlled. This was necessary as other authors have demonstrated significant differences in sensitivity of PBXs due to differences in the energetic material chemistry[58-60]. First, the polymer binder was mixed by hand for two minutes before

being added to HMX particles (BAE Systems Grade B, Class 3) and stirred by hand for two more minutes. **Table 3.1** shows the binder materials used. The mixture was then transferred to a container for mixing in a Resodyne LabRAM under vacuum for two minutes at 60% intensity. In order to make repeatable and consistent samples, a thin layer approximately 1 mm in thickness was cast into a polytetrafluoroethylene (PTFE) mold and allowed to cure for either 24 or 168 hours for Sylgard (polydimethylsiloxane) or HTPB. HTPB was cured using isophorone diisocyanate (IPDI). HTPB with a higher elastic modulus was obtained using 1,4-butanediol (BDO). Once the samples were removed from the oven, 5 mm diameter cylinders were cut from the cured layer using a hole punch.

Table 3.1: Polymer matrix components by parts for impact experiments

| Polymer Blend | Sylgard 184 Base | Sylgard 184 Curative | Sylgard 527 Base | Sylgard 527 Curative | HTPB Base | IPDI | BDO |
|---|---|---|---|---|---|---|---|
| Sylgard 5:1 | 5 | 1 | - | - | - | - | - |
| Sylgard 15:1 | 15 | 1 | - | - | - | - | - |
| Sylgard 184/527 25% | 10 | 1 | 16.5 | 16.5 | - | - | - |
| Sylgard 184/527 41% | 10 | 1 | 7.9 | 7.9 | - | - | - |
| HTPB | - | - | - | - | 10.2 | 1 | - |
| HTPB BDO | - | - | - | - | 5 | 3 | 1 |

## 3.2 Work of Adhesion and Elastic Modulus Measurement

The works of adhesion for the polymer binders were calculated by first evaluating the surface energies of the respective components using advancing stable contact angle experiments wherein water and ethylene glycol were utilized as the liquid phase atop the Sylgard 184 or HTPB solid phases. For each liquid, 6 drops of 1.5 mL were placed upon the cured polymer surface and the contact angles for each drop were measured 3 times for a total of 18 measurements per solid-liquid pairing. A Ramé-Hart advanced goniometer model 500-00 and corresponding angle

measurement software, DROPimage Advanced 2.8.03, were used to measure the contact angle formed between the liquid drop and solid surface.

The elastic modulus was determined via tensile tests on a TA Instruments DMA Q800 using film tension clamps. Samples of each material were cast into 2 mm thick flat plates and cured for 24 or 168 hrs for Sylgard and HTPB. Three rectangular samples were cut from these plates and measured using a digital caliper. Stress and strain were calculated from the load and travel distance from the tensile tester. The elastic modulus was obtained from the slope of the linear region located within the first 2% strain of the corresponding stress-strain plot.

### 3.3 Drop Weight Impact Statistical Software

The statistical test utilized here for rapid determination of the drop height sensitivity of explosives was the Neyer D-optimal test [56, 61]. This statistical test was designed to determine the most efficient testing level for sequential sampling based on the go or no-go responses of previous samples. The commercial program SenTest$^{TM}$ utilizes this test to rapidly determine the height at which 50% of the samples are expected to react, here referred to as the 50% drop height. The program also calculates maximum likelihood estimates and confidence regions of the mean (50% drop height), standard deviation, and requested response levels. The results from these tests can then be used to compare the sensitivities of a wide range of energetic materials and compositions. However, due to differences in the design of impact machines, ideally these measures should be generated for each material of interest on the same machine.

### 3.4 Drop Weight Impact Testing

The drop weight impact apparatus as depicted in **Figure 3.1** consists of a 2-meter-tall drop tower with an anvil on which the sample was placed and a guide-rail for the 5 kg drop weight trajectory. An electromagnet energized by a power supply was used to keep the weight suspended at the chosen drop height. The drop height was determined using the Neyer Sentest$^{TM}$ and was updated after each sample test. A particular variant of the drop weight impact test, the German Bundesanstalt für Materialprufung (BAM) impact test, was utilized in order to minimize variability in excitation due to divergent designs of the drop tower apparatus. In this variant, the sample was

enclosed between two metal cylinders which are placed into a metal guide ring, as shown in **Figure 3.2.** The same cylinders and guide ring were used for all tests without any grit paper.

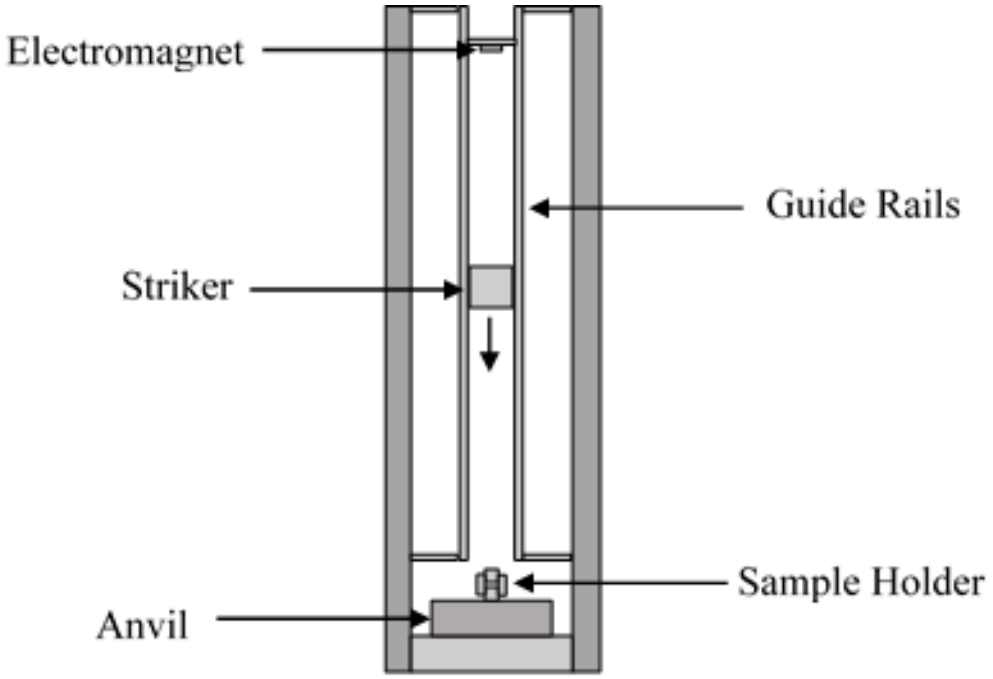


Figure 3.1: Drop weight tower schematic

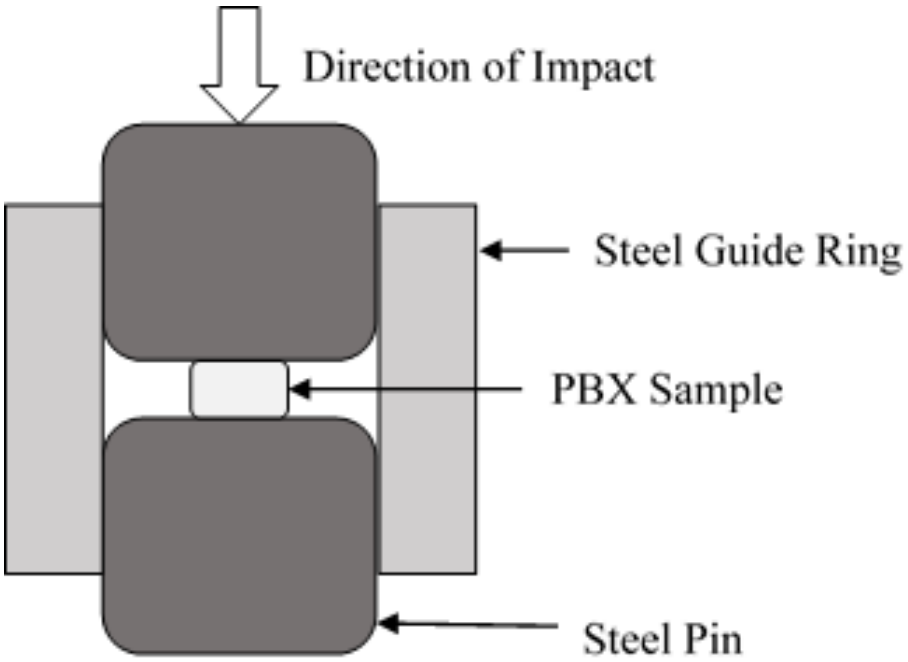


Figure 3.2: BAM impact test sample holder.

This sample holder was placed on the anvil such that the drop weight would strike the top cylinder of the sample holder. This crushes the sample as the top cylinder moves down and imparts its energy. In this way, the nature of the impact wave and the contact between the metal components and samples are similar, even across different machines. A 'go' event was indicated by a noticeable generation of a sound beyond that which was produced by impact of an inert sample, a flash as the sample combusts, or odor due to combustion products. As the samples were of appreciable size, no samples were observed to have undergone a decomposition event without immediate and obvious signs of combustion.

While the Neyer's SenTest provides estimates of a material's 50% drop height and a drop height at which to test, it does not indicate when a sufficient number of experiments have been run. The approach utilized here involved testing until the estimate of the standard deviation of the probability of reaction monotonically decreased over the course of ten tests. This generally resulted in 15-25 shots per sample type. In order to facilitate easy comparison to other drop test systems and experimental results, the estimated drop heights are also converted to drop energy.

### 3.5 Results

During testing it became clear that utilizing a BAM impact setup necessarily requires careful selection of a sufficiently small sample size in order to avoid extreme variability and increases in the drop height due to the sample deforming to the walls and significantly affecting the deformation and therefore reaction. When samples exceeded a mass of approximately 30 mg, PBX samples could fail to react even at heights in excess of 2 m. This usually led to drop heights that were clearly not indicative of the true sensitivity with estimates of the standard deviation of the drop height often exceeding 1 m. No-go experiments often resulted in seizing of the cylinders and a significantly deformed final sample. The sample appeared to have deformed to the walls of the guide ring and into the gap between the guide ring and pins. This was interpreted as being the cause of the cylinders seizing and the spurious drop heights. Effectively, most of the energy of the striker for larger samples was then being transformed into elastic deformation of the machine rather than elastic and plastic deformation of the sample. By reducing the sample size, consistent drop heights could be obtained and the corresponding standard deviations significantly decreased to a small fraction of the drop heights. This initial process of refining the testing procedure also

demonstrated that the use of new sample holders did not significantly impact the determination of the drop heights.

The experimental results for several different polymer blends are displayed in **Figure 3.3** as probability plots and **Figure 3.4** as cumulative probability plots based on the estimated drop energy, standard deviation, and an assumed normal distribution. Primarily of interest was the 50% probability of reaction which demonstrates a generally increasing required drop energy as the polymer blend becomes less pliable. Reading from 0 J to 40 J at the 0.5 probability of explosion level, the materials go from the greatest to the smallest modulus. While the differences in drop weight energy were small at elastic moduli greater than approximately 3 MPa as represented by the 5:1 samples, there was a dramatic increase in the required drop energy below this critical value. The shapes and widths of the curves reflect the estimated standard deviation of the drop energy required of the material to react. While most demonstrate a relatively sharp slope and thus a smaller standard deviation, the Sylgard 15:1 blend has a much shallower slope and thus a larger standard deviation. This was possibly due to localized inhomogeneity in the curing of the polymer due to the smaller amount of curative included in the formulation. Such disparate degrees of curing would be reflected in localized material properties including the elastic modulus. Appropriately, it would be expected that the sensitivity parameters of such a material would lie somewhere between a fully cured sample and a homogeneous partially cured sample. Based on the data collected, this blend of properties likely resulted in a wider range of responses and larger estimated standard deviation.

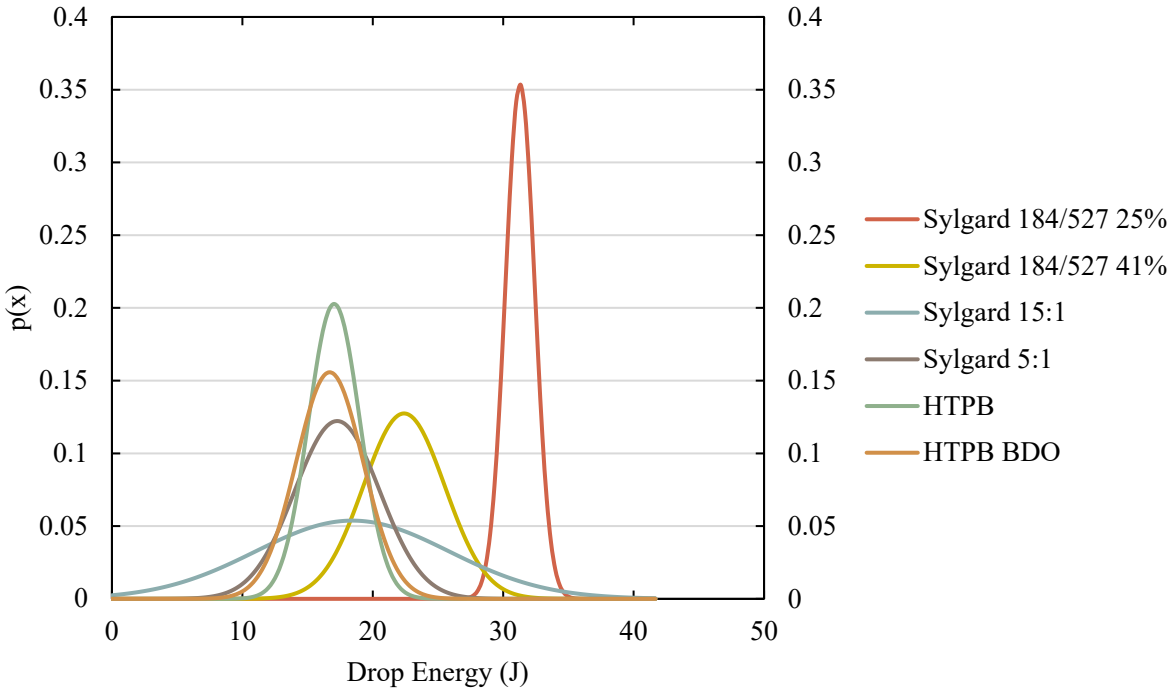


Figure 3.3: Probability density functions as a function of the drop energy input

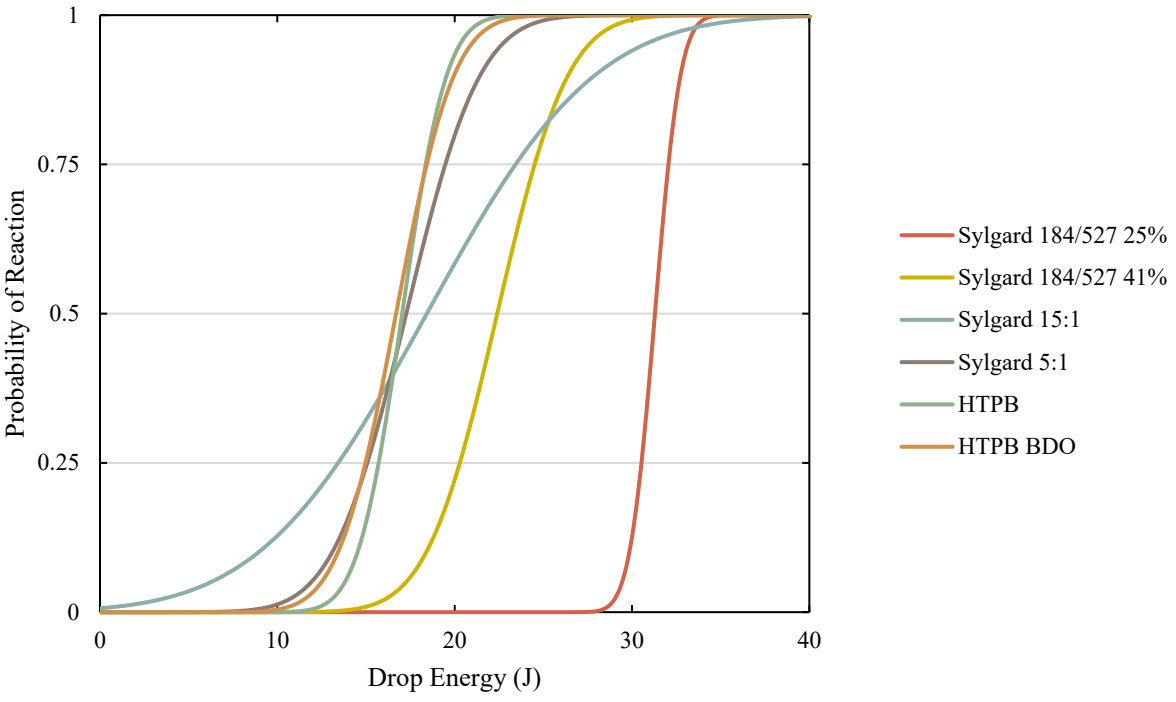


Figure 3.4: Cumulative probability of reaction as a function of drop energy input

By plotting the observed drop energy against the elastic modulus as in **Figure 3.5**, the inverse correlation between the drop energy and the elastic modulus becomes clear. Note that the error bars in **Figure 3.6** represent the Standard Error (*SE*) of the 50% drop height, as calculated using,

$$SE = \frac{s}{\sqrt{n}} \tag{3.1}$$

where *s* was the sample standard deviation, and *n* was the number of drop weight tests performed on that sample type[62]. One interpretation of the data may suggest that a logarithmic or power law model may be appropriate for correlating drop energies with binder elastic modulus. Such a curve could prove very useful for designing composites with a desired sensitivity, and also may suggest that only materials below a particular elastic modulus are appropriate for further exploration when designing energetic materials for resilience to low-speed impacts. Another interpretation of this data was that there was an elastic modulus threshold below which the drop height was extremely sensitive to modulus and above which it was relatively insensitive to this parameter.

In **Figure 3.6,** drop weight energy was plotted against the work of adhesion between the polymer and the HMX particle. A similar pattern was observed to the elastic modulus data, where significant changes in drop energy occur at the lower values of the work of adhesion and there was relatively little effect of work of adhesion on the drop energy above a threshold value. Further exploration of this particular parameter space may reveal the controlling behavior to be heavily dependent on a singular property or balance of properties. However, a qualitative comparison of the trends suggests that the elastic modulus may have a more important role in the sensitivity responses of the PBX samples. This was primarily based on the observation that the drop energy of the Sylgard PBXs varies significantly despite possessing effectively identical works of adhesion. In contrast, the variation in drop energy as a function of elastic modulus occurs over a clear range of elastic moduli. The range of these material properties can be quickly and easily understood by plotting them on an Ashby diagram as in **Figure 3.7** where the center of each polymer blend represents the mean of each property. The radii of the ellipses give the standard error of each material property.

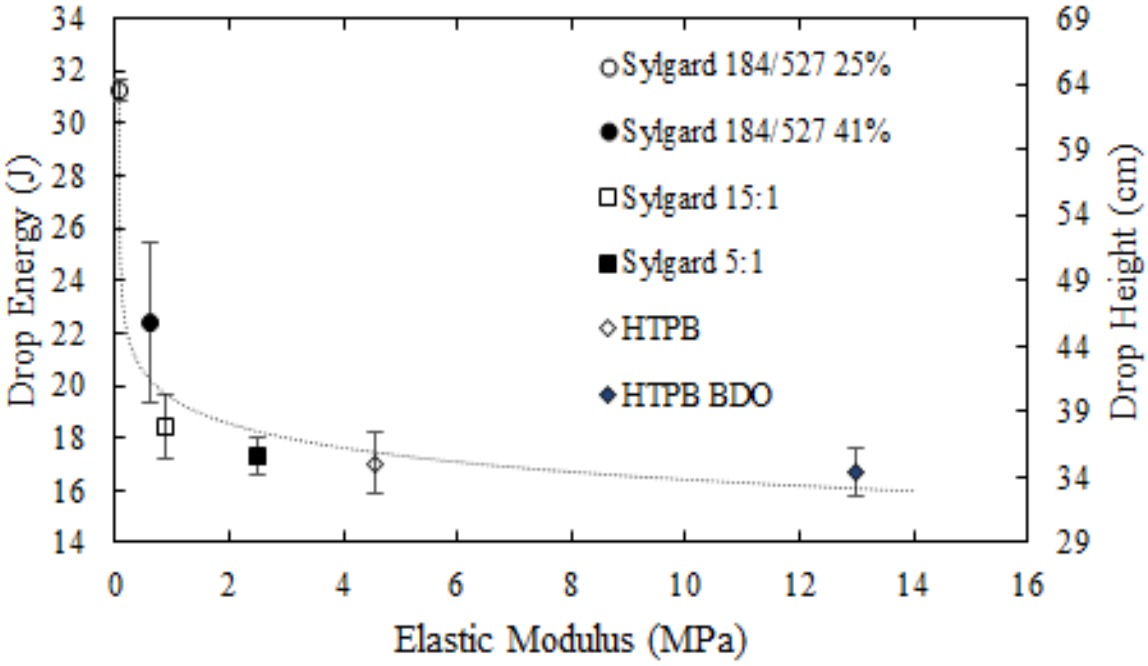


Figure 3.5: Drop energy as a function of modulus with error bars which represent the standard error of the 50% drop height.

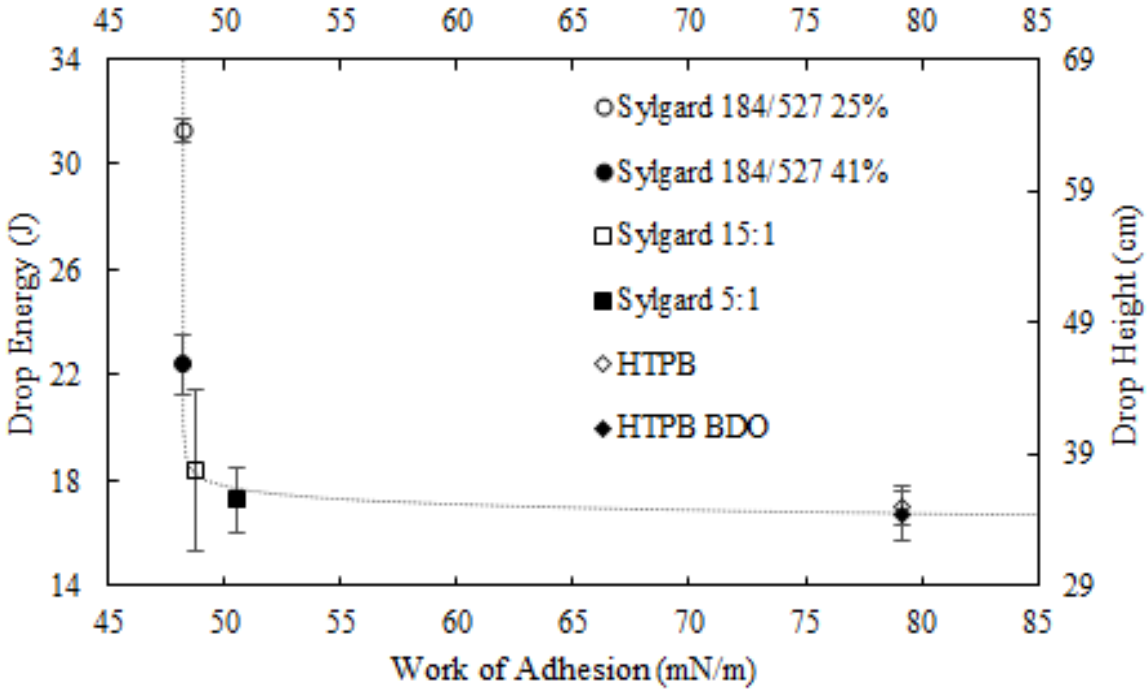


Figure 3.6: Drop energy as a function of work of adhesion with error bars which represent the standard error of the 50% drop height

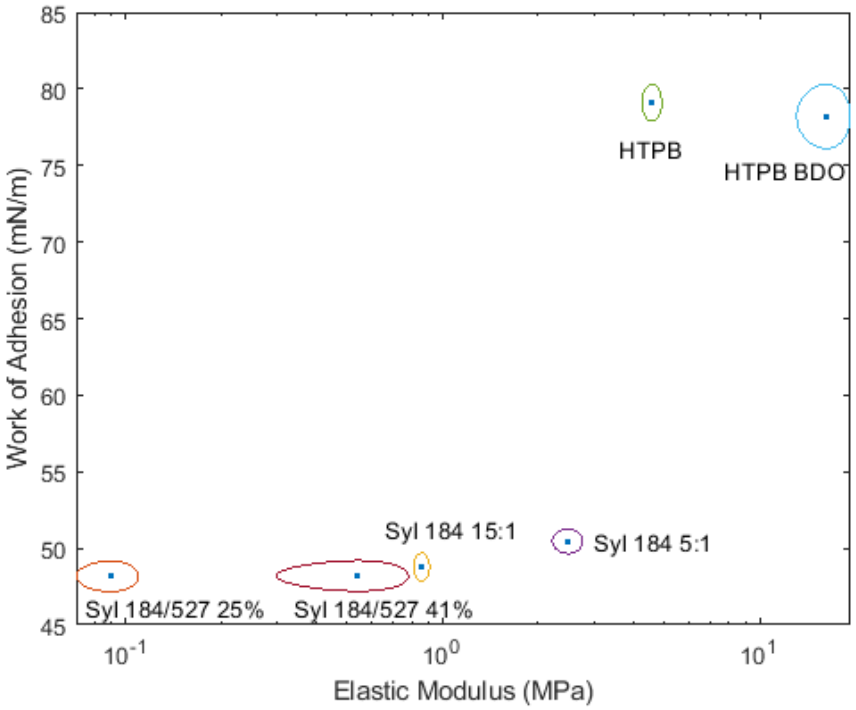


Figure 3.7: Elastic modulus and work of adhesion for selected materials

The influence of these properties was difficult to properly untangle due to the overlaps in elastic modulus and work of adhesion, but the data collected here does allow for some insight. Surfaces with a high work of adhesion will strongly adhere to each other while surfaces with a low work of adhesion will be easy to separate. A material with a high elastic modulus requires a large amount of energy to elastically deform while a material with a low elastic modulus requires very little energy to elastically deform.

During the impact experiment where the sample was undergoing compression, the binder and crystal materials are pushed closer together. Thus, more binder-air or crystal-air interfaces are not being created and such interfaces already present in the material would be eliminated creating binder-crystal interfaces. As there was no repulsion between the crystal and the binder, the formation of this interface was energetically favorable. Consequently, the work of adhesion should not have a strong effect on this kind of experiment. This was particularly clear in the case of the Sylgard 5:1 sample where the work of adhesion was low, but the elastic modulus was relatively high. The drop energy tracks with the modulus rather than with the work of adhesion. The elastic modulus influences how much of the energy from the impact was transferred to the crystal-binder

interface. If the binder was not sufficiently deformed, the bulk of the impact energy will be passed to the crystal surface allowing for relative motion and damage to the crystal, leading to hot spots. If the energy can be used to deform the bulk binder, then less energy will be passed onto the crystal interface. Thus, more overall energy was likely to be required in order to cause softer materials to generate sufficient hot spots for reaction under drop weight impact.

## 3.6 Conclusions

The work presented herein has suggested that there was value in considering low elastic modulus (<1 MPa) polymers as PBX binders. We find here, for the materials considered, a decreasing modulus results in a significant decrease in the impact sensitivity of an HMX PBX. This was in contrast to the work of adhesion which does not appear to have a significant influence on the impact sensitivity. Future work should focus on the much smaller range of material properties where the most interesting behavior was seen. Ideally, this would include materials with elastic moduli between 0.01 and 5 MPa which explores the region with the most dramatic change in impact sensitivity as well as the transition to a region where further increases in elastic modulus do not significantly influence the impact sensitivity of the PBX. While this study supports the conclusion that the elastic modulus dominates impact sensitivity behavior in this range, further study could provide valuable insight linking these properties to a specific mechanism of failure. Modifications of the experimental apparatus to allow for the capture of high-speed footage may also prove useful for determining the interplay between these properties as well as any novel phenomenon that may be responsible for the new impact behavior at the extremes of these material properties and exploiting that understanding in the design of safer PBXs.

# 4. THE ROLE OF BINDER ADHESION AND STIFFNESS IN HOT SPOT FORMATION IN ULTRASONICALLY EXCITED COMPOSITE ENERGETIC MATERIALS

The role of adhesion in the thermomechanical response of composite energetic materials under ultrasonic excitation is an area that has not been well studied. A number of previous studies have explored some aspects of this kind of excitation with particular attention paid to the thermomechanical mechanism responsible for transforming the vibration energy to thermal energy [8, 9, 11-15]. These studies have established that the frictional interaction at the interface is likely responsible for the characteristic concentration and dispersion of energy as seen in these ultrasonically-excited samples. Consequently, understanding the role of adhesion, an interfacial phenomenon, in the thermal dissipation of that ultrasonic energy could provide valuable insight into hot spot formation.

The objective of this chapter is to explore the relationship between adhesion and the heating of PBXs due to ultrasonic excitation. This work approached this question by utilizing a single crystal encased in various blocks of polymer as the test sample. These samples were excited with an ultrasonic transducer and heating at the top surface was captured with infrared thermography. For select samples, a compressive load was applied using tweezers to induce mechanical delamination in the region of the crystal-binder interface. Binder properties were varied in order to systematically alter the adhesive and mechanical properties of the sample. Portions of this chapter are reproduced from "The Role of Binder Adhesion and Stiffness in Hot Spot Formation in Ultrasonically Excited Composite Energetic Materials", which at the time of this writing has been submitted to the Journal of Applied Physics, with permission of AIP Publishing.

## 4.1 Sample Fabrication

Samples were cured in a two-step curing process in order to encapsulate a crystal in a polymer block at a depth of 1 mm from the top surface of the sample. The energetic inclusions were β-HMX crystals (BAE Systems Grade B, Class 3) sieved to only include particles between 500-850 μm. Various polymer formulations and blends were utilized in order to vary the mechanical and adhesive properties of the binder. Sylgard 184 served as a useful and versatile polymer for providing optical transparency, low adhesive strength, and easy modification of

physical properties. Utilizing Sylgard 184 also allowed for direct comparison to previous work [8, 14, 18]. Sylgard 184 was cured at 5:1, 10:1, and 15:1 base to curative ratios by weight in order to vary the mechanical strength of the binder. Sylgard 184/527 was created by mixing Sylgard 184 and Sylgard 527 at a 1:3 ratio by weight in order to produce a very compliant binder [63]. HTPB R45M HTLO was also utilized in order to compare the effects of adhesion and elastic modulus on the generation of hot spots. HTPB was cured with diisocyanate in order to achieve an isocyanate to polyol molar ratio (NCO/OH) of 1.05. Stiffer HTPB (HTPB:BDO) was produced via the addition of 1,4-butanediol (BDO) at a 5:1 molar ratio and isophorone diisocyanate (IPDI) curative was added to achieve a 1.00 NCO/OH ratio [42]. This mixture was based on the following equation for mixing ratios where *m* was mass in grams, *f* was functionality in moles of functional groups per mole of component, *M* was molar mass in grams per mole, *NCO* represents the curative IPDI, *OH* represents the additive BDO, and *HTPB* represents HTPB.

$$m_{NCO}\frac{f_{NCO}}{M_{NCO}} = m_{HTPB}\frac{f_{HTPB}}{M_{HTPB}} + m_{OH} \tag{4.1}$$

Together, these polymer blends allowed for variation of the stiffness over an order of magnitude and variation of the work of adhesion by approximately a factor of 2. The work of adhesion was chosen to describe the adhesion force between the HMX and the various polymers. The work of adhesion was quantified via contact angle measurements. **Table 4.1** explicitly shows the mass ratios used for each polymer blend. For each polymer sample, a polytetrafluoroethylene (PTFE) mold was utilized to hold a 1 mm base layer of the polymer of interest. This layer was degassed under vacuum (approximately 90 kPa below atmospheric pressure) and allowed to cure at 60 °C for 24 hr for Sylgard and 48 hr for HTPB. After the layer was cured, the inclusions were placed on the surface of the 1 mm layer before another 4 mm layer of liquid polymer was poured over the crystals and the samples were again degassed under vacuum. The Sylgard samples were allowed to cure for an additional 24 hr at 60 °C while the HTPB samples were cured for 7 days at 60 °C. These samples were then removed from the mold and rectangular cross-sections of 5 mm x 5 mm were cut out using a razor blade to yield a rectangular prism of polymer containing a single crystal set 1 mm away from the top surface. Delaminated samples were created by subjecting the cured samples to mechanical stress until debonding was observed via a Hirox KH-8700 microscope across at least half of the inclusion's surface.

Table 4.1: Polymer matrix components by parts for the ultrasonic experiments

| Polymer Blend | Sylgard 184 Base | Sylgard 184 Curative | Sylgard 527 Base | Sylgard 527 Curative | HTPB Base | IPDI | BDO |
|---|---|---|---|---|---|---|---|
| Sylgard 5:1 | 5 | 1 | | | | | |
| Sylgard 15:1 | 15 | 1 | | | | | |
| Sylgard 184/527 | 9.8 | 1 | 16.3 | 16.3 | | | |
| HTPB | | | | | 10.2 | 1 | |
| HTPB BDO | | | | | 6.2 | 3.1 | 1 |

## 4.2 Excitation and Measurement

A Steiner & Martins, Inc. SMD10TR111 piezoelectric ultrasonic transducer was used to excite all of the samples to allow for comparison to earlier works. In order to ensure good contact and mechanical coupling between the sample and the transducer, Sonotech Soundsafe ultrasonic coupling agent was applied between the sample and the transducer. Care was taken to ensure that the coupling agent was uniformly applied and that there was good contact between the polymer surface and ultrasonic transducer. After each excitation, the samples underwent a 5 min rest period to allow for the sample and transducer to relax and return to ambient temperatures.

The transducer was excited for 4 s with a sinusoidal signal from an Agilent N9310A RF signal generator (210.5 kHz at -3.0 dBm) and amplified by a Mini-Circuits LZY-22+ high power amplifier (+43 dB, 24 V power supplied from a Keysight E3634A DC power supply) yielding 10 W of electrical power. A frequency of 210.5 kHz for the excitation signal was chosen as it was near the resonant frequency of the transducer and previous studies have shown that this frequency resulted in a maximum temperature rise due to interfacial interactions with the inclusion [8]. The excitation time of 4 s was utilized in order to study the immediate responses of the sample and allow for multiple uses of the same sample without risking decomposition of the energetic inclusion. The excitation time was monitored with a Tektronix DPO 4043 oscilloscope. The temperature at the top of the polymer surface was captured with a FLIR A325sc infrared camera paired with a FLIR T197200 close-up 2x lens recording at 30 Hz (see **Figure 4.1**). The starting frame was determined via the immediate Ohmic heating of the wire leads connected to the

transducer. Temperature sensitivity was reported by the manufacturer to be 0.07 °C at 30 °C with an accuracy of ±2 °C or ±2% of the reading.

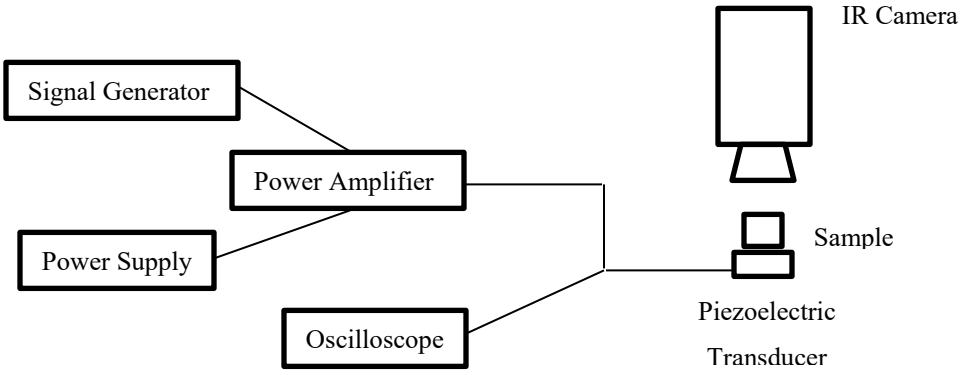


Figure 4.1: Experimental apparatus used to apply ultrasonic energy to the composite materials and to monitor the resulting temperature change

## 4.3 Work of Adhesion and Elastic Modulus Measurement

In order to provide a quantitative measure of the adhesive forces between the polymer binder and HMX inclusion, the work of adhesion was chosen as a metric. The thermodynamic work of adhesion was the increase in free energy as two surfaces are separated. This can be calculated from the surface energies of each of the materials of interest. The surface energies can be determined using contact angle experiments wherein the angle between a liquid and solid in contact was measured. This approach was utilized previously in order to determine the relationship between the work of adhesion and the drop weight sensitivity of a PBX [57]. Similarly, the elastic modulus was determined in the same work via tensile testing.

## 4.4 Heat Generation Rate and Density Measurement

In order to determine the heat generation rate, the following equation utilized by Mares *et al.* was employed [8],

$$T_s(t) = \frac{q}{2\pi kd} erfc\left(\frac{d}{\sqrt{4\alpha t}}\right) \tag{4.2}$$

**Equation 4.2** describes the surface temperature directly above a point heat source in a semi-infinite plane. The heat generation rate in Watts, $q$, was assumed to be constant and the depth of the point heat source in meters, $d$, was taken to be the distance from the top surface to the middle of the

particle inclusion. Coupled with the thermal conductivity in Watts per meter-Kelvin, $k$, and the thermal diffusivity in square meters per second, $\alpha$, time-temperature data can be used to find the heat generation rate. The primary weakness of this model was a particular sensitivity to the heat source depth, as all of the other variables can be measured to a reasonable degree of accuracy. Thus, it was insufficient to utilize only the average particle size for predicting the constant heat generation rate. To address this concern, each particle embedded in the polymer was measured using a Hirox KH-8700 digital microscope after encapsulation. Given the short excitation and measurement times, this model was deemed appropriate for determining the temperatures at the crystal surface, as well as the heating rate. The short excitation times also reduced deviation from the model due to phenomena such as cooling at the interfaces, changes in material properties due to an increase in temperature, and edge effects due to the finite size of the samples.

## 4.5 Results

The heat generation rates at the HMX particle embedded in each polymer material due to ultrasonic excitation for 4 s are shown as box and whisker plots in **Figure 4.2**. The plots were built from the average heat generation rate calculated from surface temperature measurements over five ultrasonic excitation experiments on each of the 17 samples studied. There was a clear difference between the undamaged and delaminated samples, wherein the delaminated cases exhibit a much greater degree of heating.

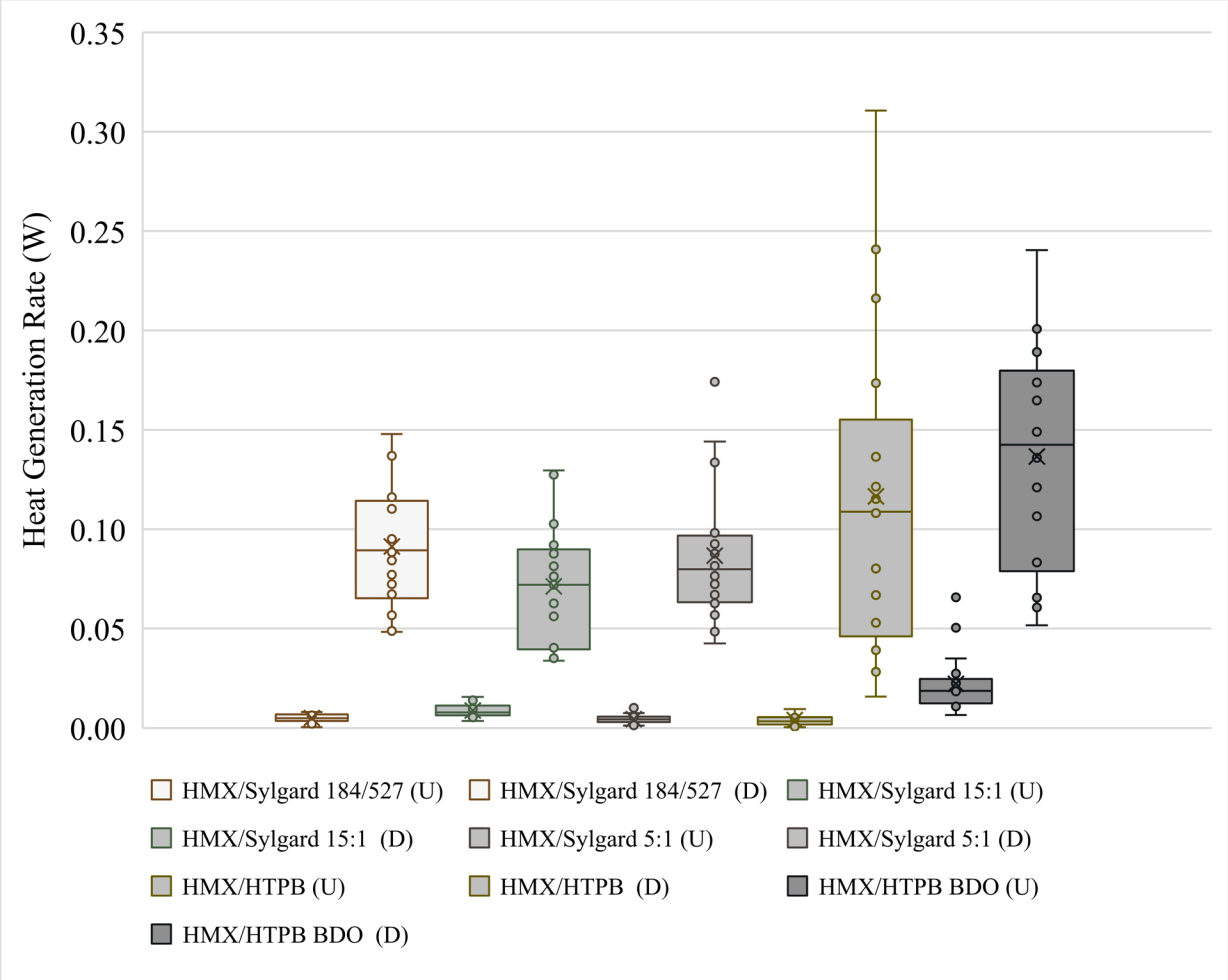


Figure 4.2: Heat generation rate at the HMX particle embedded in each polymer material (D = delaminated samples; U = undelaminated samples)

For the undamaged material, the heating patterns observed can generally be described as a low-level bulk heating with no concentration of thermal energy and can be attributed to viscoelastic dissipation, as seen in earlier literature [15]. This generally appears as seen in **Figure 4.3** where the heating due to ultrasonic excitation can be seen as generally even and low intensity across the entirety of the top surface.

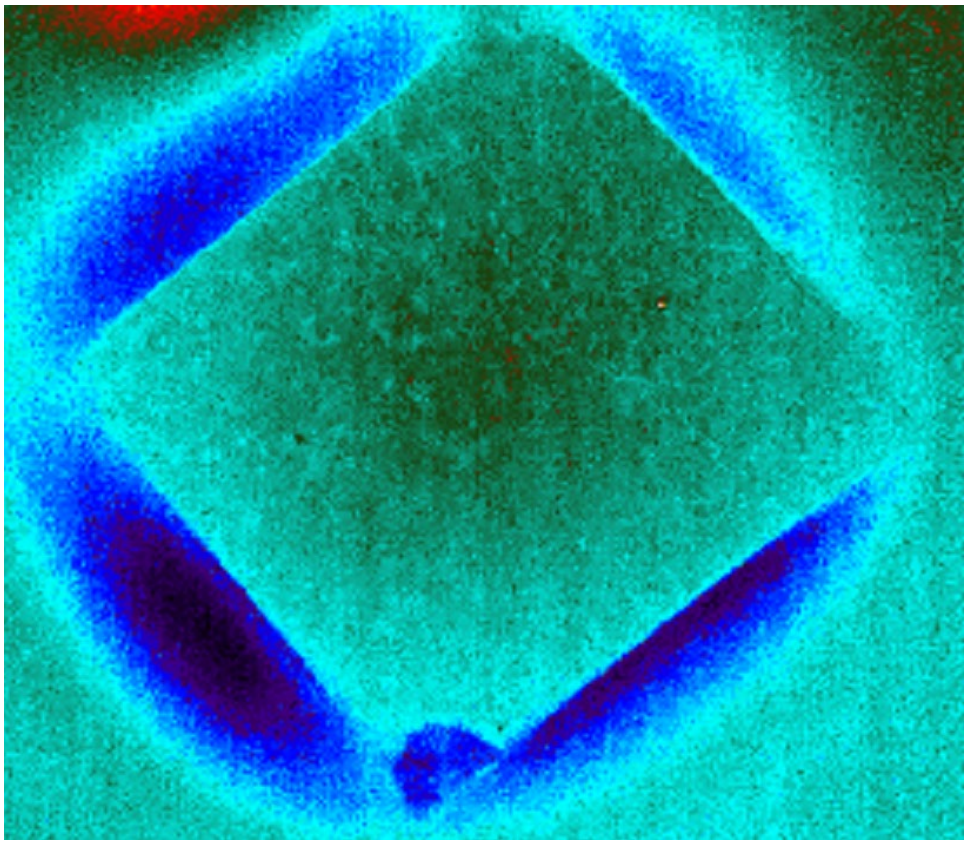

Figure 4.3: Even heating pattern on top surface of undamaged sample

For the mechanically delaminated case, a higher degree of heating and a characteristic circular heating pattern above the crystal inclusion were observed which was attributed to frictional dissipation at the crystal interface and subsequent conduction through the polymer binder. An example of this circular heating pattern is shown in **Figure 4.4**.

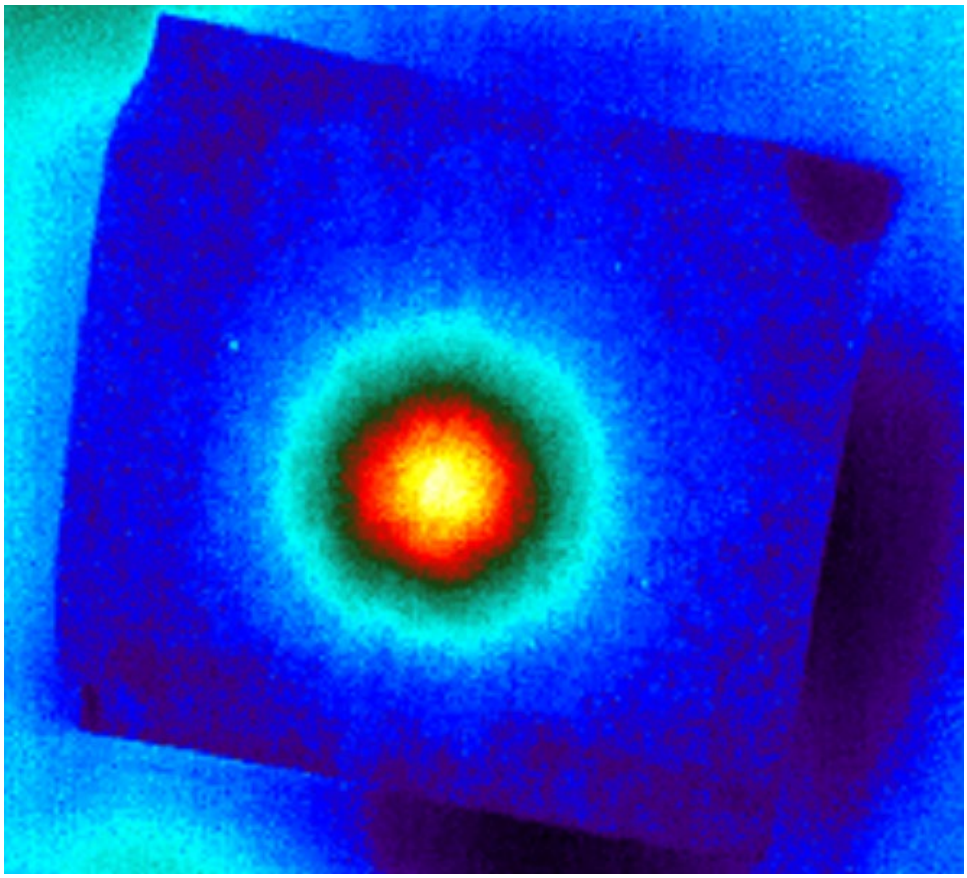

Figure 4.4: Characteristic circular heating pattern on top surface of damaged sample

This low-grade heating is captured at the top surface with a temperature trace indicative of heat conduction from the transducer and low-grade constant heating from viscoelastic dissipation occurring throughout the material. A standard example of such a temperature trace of an excited HTPB sample is shown in **Figure 4.5**. Over the course of 8 seconds, the temperature only increases by less than 1 degree Celsius.

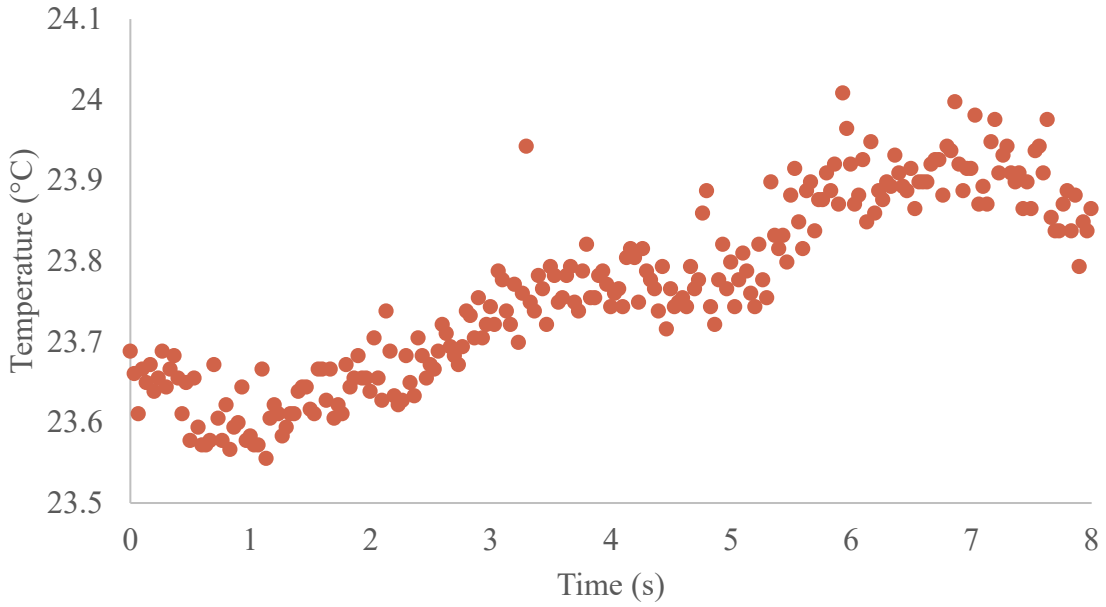


Figure 4.5: Temperature trace of the top surface of an undamaged HTPB sample

These patterns were consistent across polymer blends as long as delamination had not occurred and can be seen in **Figure 4.6** with a Sylgard sample.

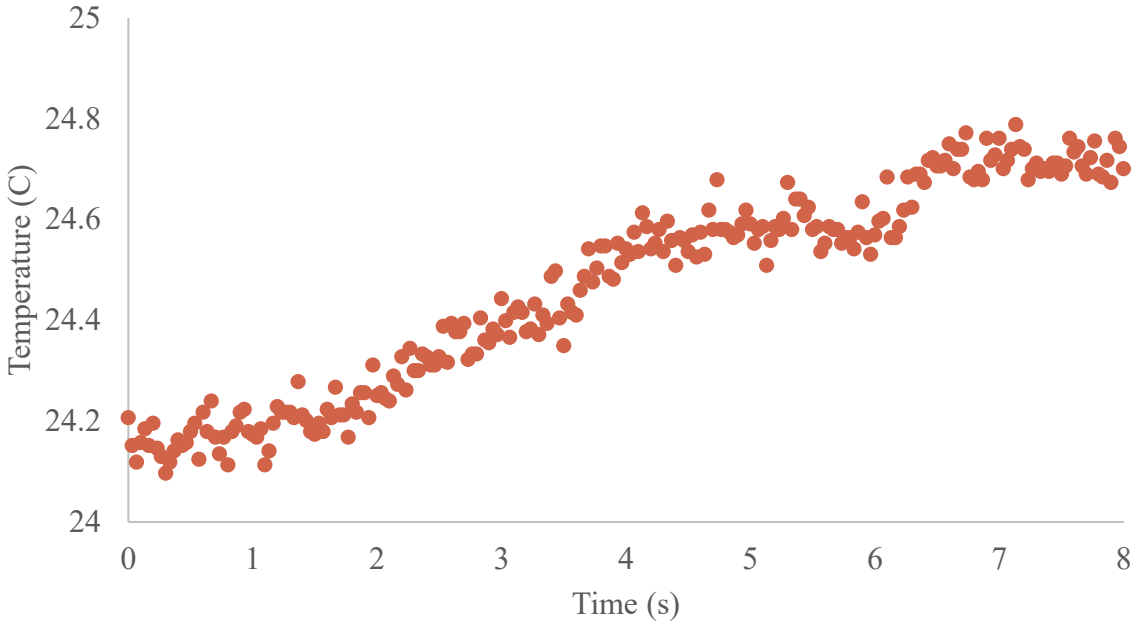


Figure 4.6: Temperature trace of the top surface of an undamaged HTPB sample

An example of the temperature trace for this material can be seen in **Figure 4.7** which is characterized by a marked increase in heating at a relatively constant rate which then drops off once excitation has ceased.

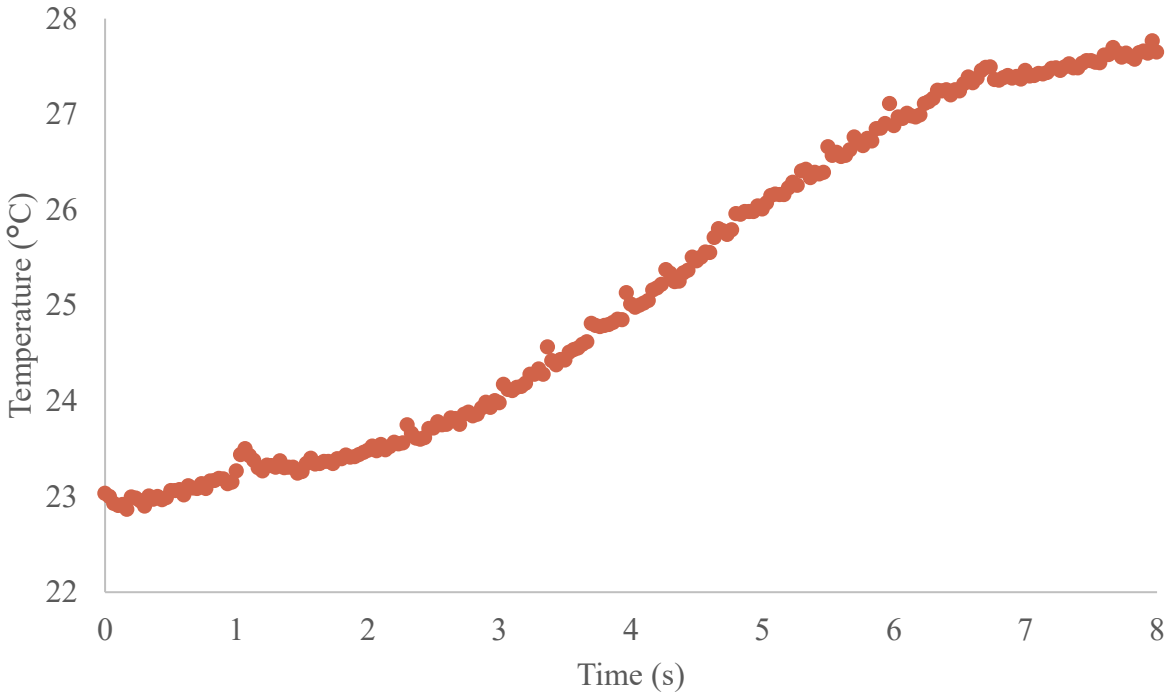


Figure 4.7: Temperature trace of the top surface of a damaged sample

These conclusions were based on the differences between the damaged and undamaged samples when delamination has occurred, as well as earlier literature which supports this interpretation [11]. The key result from literature was the direct observation of movement of the binder during ultrasonic excitation which allows for interfacial phenomena, such as surface energy, to potentially play a role in ultrasonic energy dissipation. The introduction of a moveable interface by mechanically debonding the interface before excitation allows for an investigation of how material properties influence energy dissipation at the crystal surface.

The measurements in **Table 4.2** show that the work of adhesion did not significantly change with the variation of the curative agent for Sylgard 184 or with the addition of the Sylgard 527. **Table 4.3** shows that the variation in elastic modulus in the materials with Sylgard binder covers about an order of magnitude while the HTPB mixes vary in stiffness by a factor of 3.

**Table 4.2:** Works of Adhesion with Standard Errors for Various Polymers with HMX

Table 4.2: Work of adhesion, with standard errors, for each polymer material

| | $W_A$ (mN/m) | $SE_{Wa}$ (mN/m) |
|---|---|---|
| HTPB | 79 | 1.2 |
| HTPB with BDO | 78 | 2.1 |
| Sylgard 5:1 | 51 | 0.75 |
| Sylgard 15:1 | 49 | 0.94 |
| Sylgard 184/527 | 48 | 1.0 |

Table 4.3: Elastic modulus, with standard errors, for each polymer material

| | E (MPa) | $SE_E$ (MPa) |
|---|---|---|
| HTPB | 4.6 | 0.33 |
| HTPB with BDO | 16 | 3.1 |
| Sylgard 5:1 | 2.5 | 0.27 |
| Sylgard 15:1 | 0.86 | 0.050 |
| Sylgard 184/527 | 0.090 | 0.020 |

The data presented in **Figure 4.8** demonstrates the range of elastic moduli and works of adhesion accessible by using the five selected materials. The center point of each ellipse represents the average of each property for a given material with the major and semi-major axes of the ellipses corresponding to the standard error of each property measurement. This yields five materials that allow for significant variation of modulus and work of adhesion over the range accessible by these materials. Pairing these material properties with the debonded average heat generation rate data presented in **Figure 4.9** and the findings of earlier studies [11] allows for a number of observations and conclusions to be made.

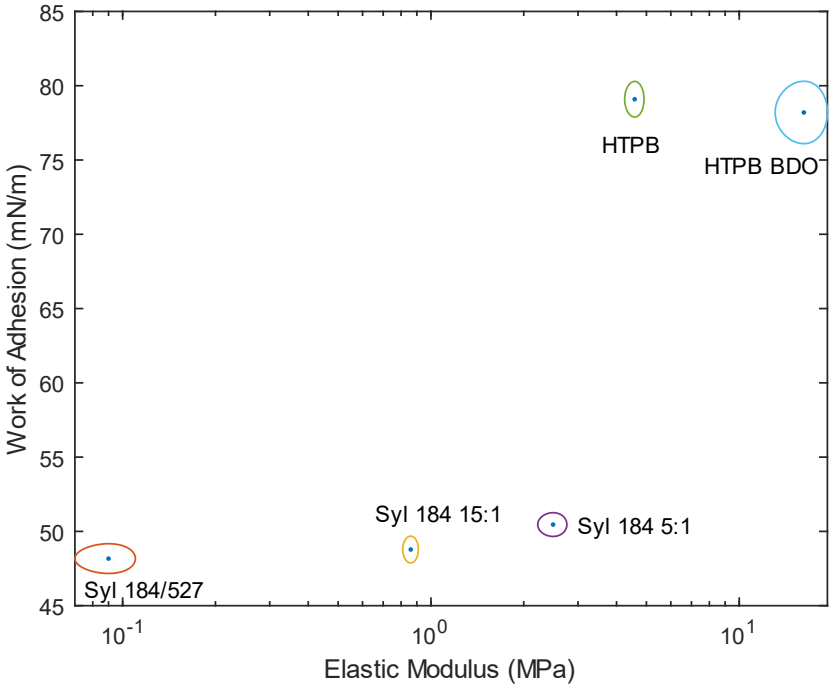


Figure 4.8: Elastic modulus and work of adhesion for selected materials

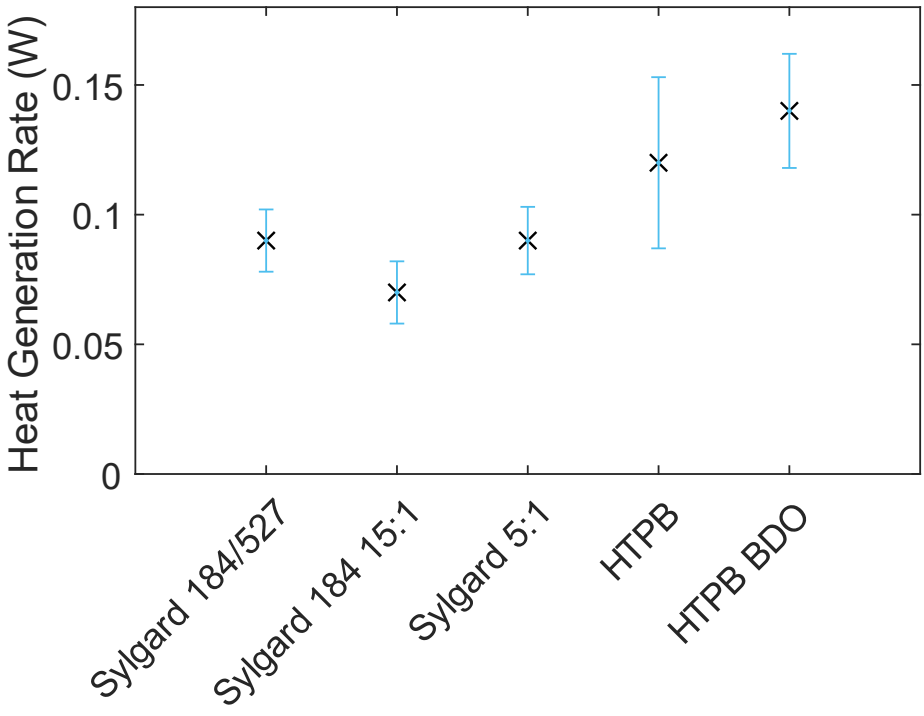


Figure 4.9: Average heat generation rate at the debonded HMX particle embedded in each polymer material.

While there were some differences between the heat generation rates of each type of sample, ultimately the evidence suggested that changing the work of adhesion or the elastic modulus over the tested ranges did not significantly change the thermomechanical behavior or degree of heating, especially compared to the changes produced by delamination. The seemingly small impact of the work of adhesion can be explained by examining the fundamental forces that are described by surface energy. Surface energy is a thermodynamic measure of the amount of energy required to separate two surfaces in molecular contact (~0.1-0.2 nm) and is a consequence of intermolecular forces, such as van der Waals and hydrogen bonding [64, 65]. As the interaction due to these electromagnetic forces decay as $r^{-6}$, surface roughness can be the most important factor in determining the effective adhesion that occurs between two real surfaces [66-69]. Given that the samples were mechanically delaminated so that intimate molecular contact was broken, the roughness of the HMX crystals and the polymer binder greatly diminished the effective adhesion forces acting between the two surfaces. Consequently, the relatively insignificant role of adhesion in the thermomechanical response of these samples under ultrasonic excitation was a result that was well described by the application of previous studies on adhesive forces.

The analysis of the role of the elastic modulus in the thermomechanical response of the samples to ultrasonic excitation was a relatively independent consideration. The variation of the elastic modulus over two orders of magnitude certainly does not introduce drastic changes in the degree of heating observed. Comparison of this data to previous studies with similar excitation parameters does not reveal a significant deviation in the degree of thermomechanical heating [18]. The most important variable for generating significant localized heating across all of the samples in this study was the introduction of delamination before excitation occurred. Once intimate contact was lost at the interface, the frictional heating occurred with effectively negligible influence from the work of adhesion or elastic modulus.

## 4.6 Conclusion

This work utilized a single inclusion-binder system to investigate the heating response of compound explosives to low energy ultrasonic excitation. These experiments were carried out with HMX inclusions in cured Sylgard or HTPB matrices. Mechanical force was applied to a subset of the samples in order to delaminate the polymer material from the inclusion. The observed heating during ultrasonic excitation showed a clear distinction between the undamaged and delaminated

cases wherein the heating observed for the delaminated cases far exceeded the heating observed in the undamaged cases. This supports the hypothesis that a key driver of heating at low excitation energies was the relative motion between the crystal and the polymer binder, which was enabled by the loss of intimate molecular contact between the inclusion and the binder. Based on the collected data and the application of previous theories on adhesion, it was evident that neither the work of adhesion nor the elastic modulus had a significant influence on the degree of thermomechanical heating in the studied frequency range if mechanical delamination had been applied. This suggested that the mechanism responsible for the localized heating was not dependent on either property as explored here. Future work should focus on exploring either heightened excitation parameters or more extreme material parameters in order to understand the thermomechanical mechanism. The conclusions presented here are the product of a simplified single crystal sample under specific excitation conditions, but this effort contributes to the body of work informing future studies and safety considerations related to the high-frequency vibration of energetic materials.

# 5. THE ROLE OF BINDER ADHESION AND STIFFNESS IN HOT SPOT FORMATION IN COMPOSITE ENERGETIC MATERIALS DUE TO STRONGLY COUPLED ULTRASONIC EXCITATION

While a number of previous studies have explored aspects of ultrasonic excitation of composite energetic materials, there is significant work remaining to be performed investigating the thermomechanical mechanism responsible for transforming vibrational energy to thermal energy in these materials [8, 9, 11-15]. These previous studies have established that frictional interactions at the interface are likely responsible for the characteristic concentration and dispersion of energy during ultrasonic-excitation of PBXs. Understanding the role of adhesion, an interfacial phenomenon, in the thermal dissipation of that ultrasonic energy may provide valuable insight into hot spot formation.

The objective of this chapter is to explore the relationship between adhesion and the heating of PBXs due to strongly coupled ultrasonic excitation. This work approached this question by utilizing a single crystal encased in various blocks of polymer as the test sample. These samples were excited with an ultrasonic transducer and heating at the top surface was monitored with infrared thermography. The samples were strongly coupled to the ultrasonic transducer with ethyl cyanoacrylate. Binder properties were varied in order to systematically alter the adhesive and mechanical properties of the sample.

## 5.1 Sample Fabrication

In order to ensure individual crystals were uniformly placed within the polymer block, a two-step curing process was adopted as in earlier works. This ensured that each sample had a single energetic crystal located 1 mm below the top surface of the polymer block. The crystals were β-HMX crystals (BAE Systems Grade B, Class 3) which had been sieved to ensure that only particles between 500-850 μm were included. Hydroxyl-terminated polybutadiene (HTPB) and polydimethylsiloxane (PDMS) were selected as binders due to their widely varying mechanical and adhesive properties. For the purposes of creating an optically clear polymer blend with low adhesive strength and easily modified physical properties, Sylgard 184, a PDMS blend, was also utilized as a binder This polymer blend was often studied elsewhere, and utilizing this polymer allows for quick and direct comparison to previous work [8, 14, 18]. Modification of the

mechanical strength of the binder was achieved by curing two Sylgard 184 blends at varying curative ratios. A more compliant binder was created utilizing Sylgard 527, a PDMS blend, for creating a softer final polymer [63]. The adhesion of the polymer binder was significantly increased by using HTPB as the polymer binder. As a softer HTPB final polymer was desired in order to minimize simultaneous mechanical changes when the adhesion was increased, HTPB was cured with isophorone diisocyanate (IPDI) in order to achieve an isocyanate to polyol molar ratio (NCO/OH) of 0.8 [42]. **Table 5.1** explicitly shows the mass ratios used for each polymer blend.

Table 5.1: Polymer matrix components by parts for the ultrasonic experiments

| Polymer Blend | Sylgard 184 Base | Sylgard 184 Curative | Sylgard 527 Base | Sylgard 527 Curative | HTPB Base | IPDI | BDO |
|---|---|---|---|---|---|---|---|
| Sylgard 5:1 | 5 | 1 | | | | | |
| Sylgard 15:1 | 15 | 1 | | | | | |
| Sylgard 184/527 | 9.8 | 1 | 16.3 | 16.3 | | | |
| HTPB 0.8 | | | | | 13.4 | 1 | |

**Equation 5.1** was utilized in order to calculate the amount of HTPB base and IPDI curative necessary to achieve this molar ratio. In this equation. *m* was mass in grams, *f* was functionality in moles of functional groups per mole of component, *M* was molar mass in grams per mole, *IR* was the polyol molar ratio or index ratio, *NCO* represents the curative IPDI, *OH* represents the additive BDO, and *HTPB* represents HTPB.

$$m_{NCO}\frac{f_{NCO}}{M_{NCO}} = (IR)\left(m_{HTPB}\frac{f_{HTPB}}{M_{HTPB}} + m_{OH}\right) \tag{5.1}$$

These polymer blends allowed stiffness to vary by an order of magnitude and for the work of adhesion against HMX to vary approximately by a factor of 2. The work of adhesion was quantified via contact angle measurements as utilized in earlier works. In order to avoid damage to the samples on removal from the curing molds, a polytetrafluoroethylene (PTFE) mold was utilized to first cure the 1 mm base layer of the polymer of interest. After degassing the mixed polymer base and curative under vacuum (approximately 90 kPa below atmospheric pressure), the mixture was poured into the PTFE mold and allowed to cure at 60 °C for 24 hr for Sylgard and 48 hr for HTPB. After curing, the inclusions were placed on the surface of the 1 mm layer before

another 4 mm layer of liquid polymer was mixed and degassed. This mixture was poured over the crystals, and the samples were cured. The Sylgard samples were allowed to cure for an additional 24 hr at 60 °C while the HTPB samples were cured for 7 days at 60 °C. These samples were then removed from the mold and rectangular cross-sections of 5 mm x 5 mm were cut out using a razor blade to yield a rectangular prism of polymer containing a single crystal set 1 mm away from the top surface.

## 5.2 Excitation and Measurement

Steiner & Martins, Inc. SMD10TR111 piezoelectric ultrasonic transducers were used to excite all of the samples to allow for comparison to earlier works. In order to ensure good contact and strong mechanical coupling between the sample and the transducer, ethyl cyanoacrylate (Loctite Super Glue Gel Control) was applied between the sample and the transducer. Care was taken to ensure that the coupling agent was uniformly applied and that there was good contact between the polymer surface and ultrasonic transducer. As transducers could significantly increase to temperatures in excess of 130 °C over the course of the experiment, new transducers were required for each sample. After excitation, the adhesive between the sample and the transducer would often be damaged with clear loss of contact between the two surfaces. With some transducers, the solder could also be melted leading to the separation of the wire leads from the transducer contacts. The transducers were excited for 20 s with a sinusoidal signal from an Agilent N9310A RF signal generator (210.5 kHz at -3.0 dBm) and amplified by a Mini-Circuits LZY-22+ high power amplifier (+43 dB, 24 V power supplied from a Keysight E3634A DC power supply) yielding 10 W of electrical power. A frequency of 210.5 kHz for the excitation signal was chosen as it was near the resonant frequency of the transducer and previous studies have shown that this frequency resulted in a maximum temperature rise due to interfacial interactions with the inclusion [8]. . After 15 seconds, the ohmic heating from the transducer could significantly contribute to the heating rate near the inclusion due to thermal conduction from the transducer. While an approximate excitation time of 20 s was utilized, analysis was based on the first 15 seconds of excitation. The excitation time was monitored with a Tektronix DPO 4043 oscilloscope. The temperature at the top of the polymer surface was captured with a FLIR A325sc infrared camera paired with a FLIR T197200 close-up 2x lens recording at 30 Hz. The starting frame was determined via the immediate ohmic heating of the wire leads connected to the transducer.

Temperature sensitivity was reported by the manufacturer to be 0.07 °C at 30 °C with an accuracy of ±2 °C or ±2% of the reading.

## 5.3 Work of adhesion and elastic modulus measurement

In order to provide a quantitative measure of the adhesive forces between the polymer binder and HMX inclusion, the work of adhesion was chosen as a metric. The thermodynamic work of adhesion is the increase in free energy as two surfaces are separated. This can be calculated from the surface energies of each of the materials of interest. The surface energies can be determined using contact angle experiments wherein the angle between a liquid and solid in contact was measured. This approach was utilized previously in order to determine the relationship between the work of adhesion and the drop weight sensitivity of a PBX [57]. Similarly, the elastic modulus was determined in the same work via tensile testing.

## 5.4 Results

The maximum surface temperature recorded at the top surface of each polymer material following15 seconds of ultrasonic excitation are shown in **Figure 5.1** as box and whisker plots. The significant temperature rises at the top surface of the polymer samples were sufficient to allow evaluation of the changes in the thermomechanical mechanism. These plots were built from testing at least 13 replicates of each polymer sample, with each sample utilizing a unique transducer. Many Sylgard 184/527 and Sylgard 15:1 samples displayed localized heating at the top surface in a characteristic circular heating pattern. This particular pattern of heating has been shown in previous works to be the result of delamination occurring at the interface between the energetic crystal and the polymer material. This delamination is the loss of close intermolecular contact between the two materials. Once delamination has occurred, relative motion of the polymer binder against the energetic crystal can occur and ultrasonic energy can be transformed into thermal energy. As this interaction occurs at the interface, the heating is localized to the inclusion and a characteristic heating pattern can be seen. The temperature rises in these cases were normally far in excess of the low-level bulk heating observed in cases where no characteristic circular heating pattern was observed. The Sylgard 5:1 and HTPB samples uniformly showed no characteristic heating pattern at the top surface for any samples.

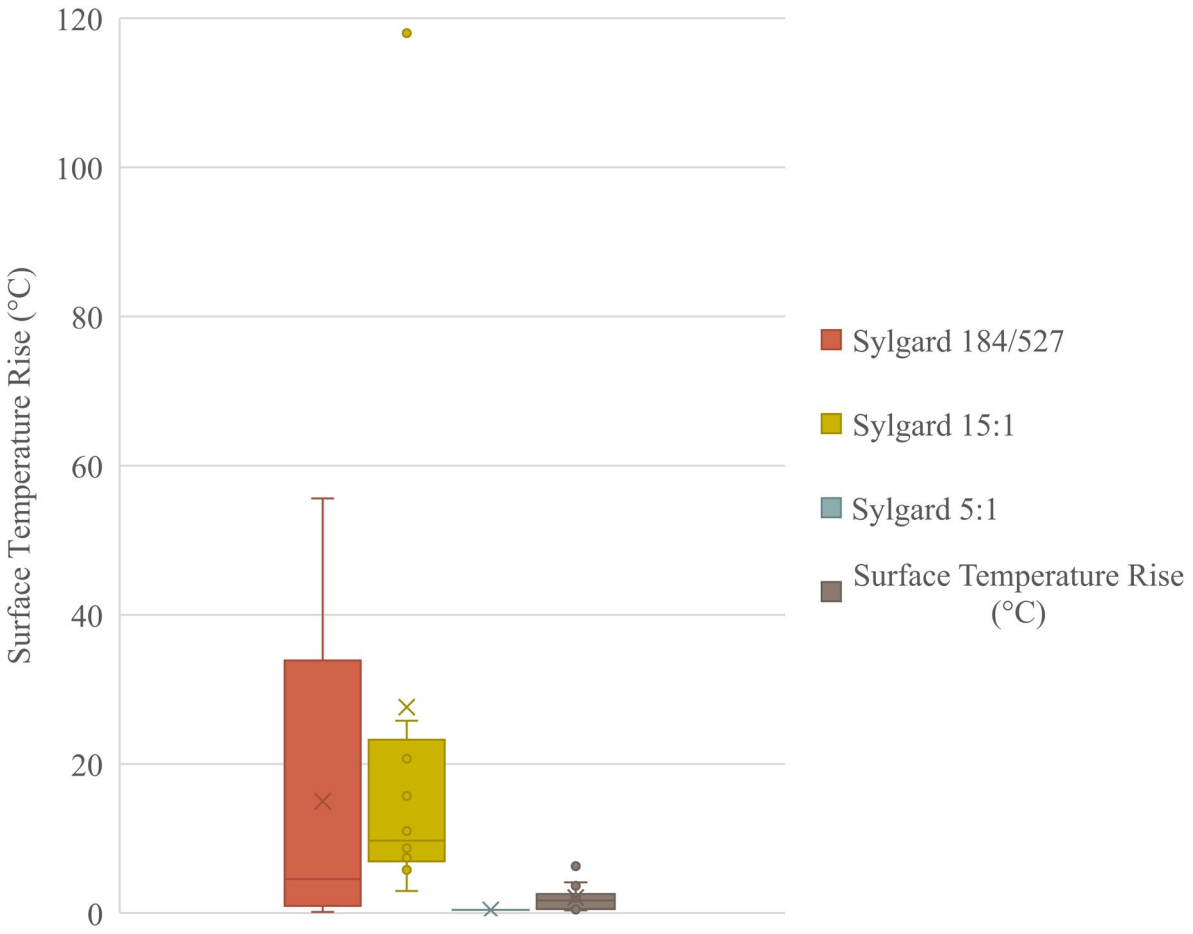


Figure 5.1: Increase of the maximum surface temperature of strongly coupled ultrasonic samples after 15 seconds

In **Figure 5.2**, the max surface temperature rise of each polymer sample type was plotted against the elastic modulus of their respective polymer blends [70]. The Sylgard blend samples, which had practically identical works of adhesion, appear to show that the elastic modulus had some impact on the thermomechanical heating mechanism. The nature and degree of this impact could not be readily ascertained from simply examining the average heating response and required examining the data as discrete maximum surface temperature rises. This was required only for the sets of polymer samples, Sylgard 184/527 and Sylgard 15:1, which had the characteristic circular heating pattern indicative of localized heating. It should also be noted that the HTPB samples did not show a localized heating response despite having a relatively low elastic modulus. This was interpreted to be due to the higher work of adhesion which prevented the loss of contact typically

responsible for allowing a frictional heating mechanism to occur at the crystal-polymer interface. This is further discussed after the analysis of the Sylgard cases.

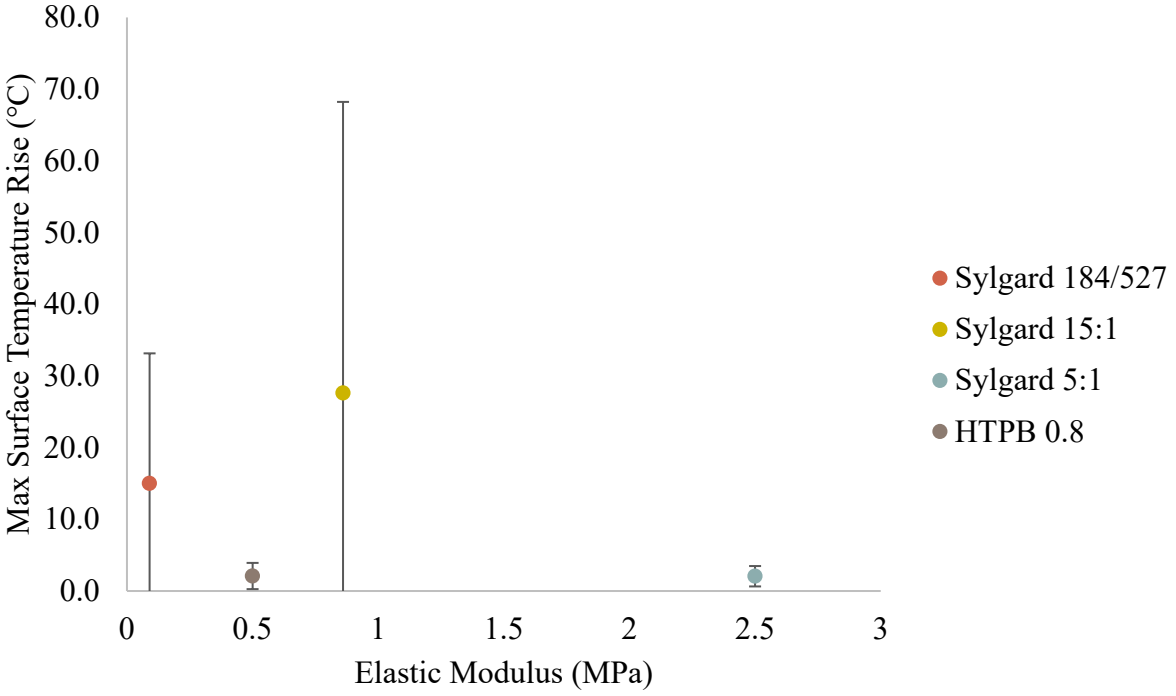


Figure 5.2: Average max surface temperature rise at the top surface of the polymer samples with standard deviations as error bars

The maximum temperature rise at the surface of each Sylgard 184/527 sample is plotted in **Figure 5.3.** These samples showed a wide range of responses, including some samples that showed a characteristic circular heating pattern (red triangles), and samples which heated uniformly (blue circles). Approximately 42% of these samples had the circular pattern indicating localized heating, and these samples ranged in the maximum surface temperature achieved from 6 °C to 56 °C. None of these samples were observed to undergo a reaction or produce significant quantities of gas. The samples had a mean maximum surface temperature rise of 32.6 °C and a median maximum surface temperature rise of 38.6 °C, demonstrating a relatively centered distribution with heating responses skewing slightly left. The behavior of the Sylgard 184/527 samples in terms of maximum surface temperature rise can be described as 42% of the samples experienced a localized heating event with 64% of these samples experiencing a maximum surface temperature rise in excess of 30 °C.

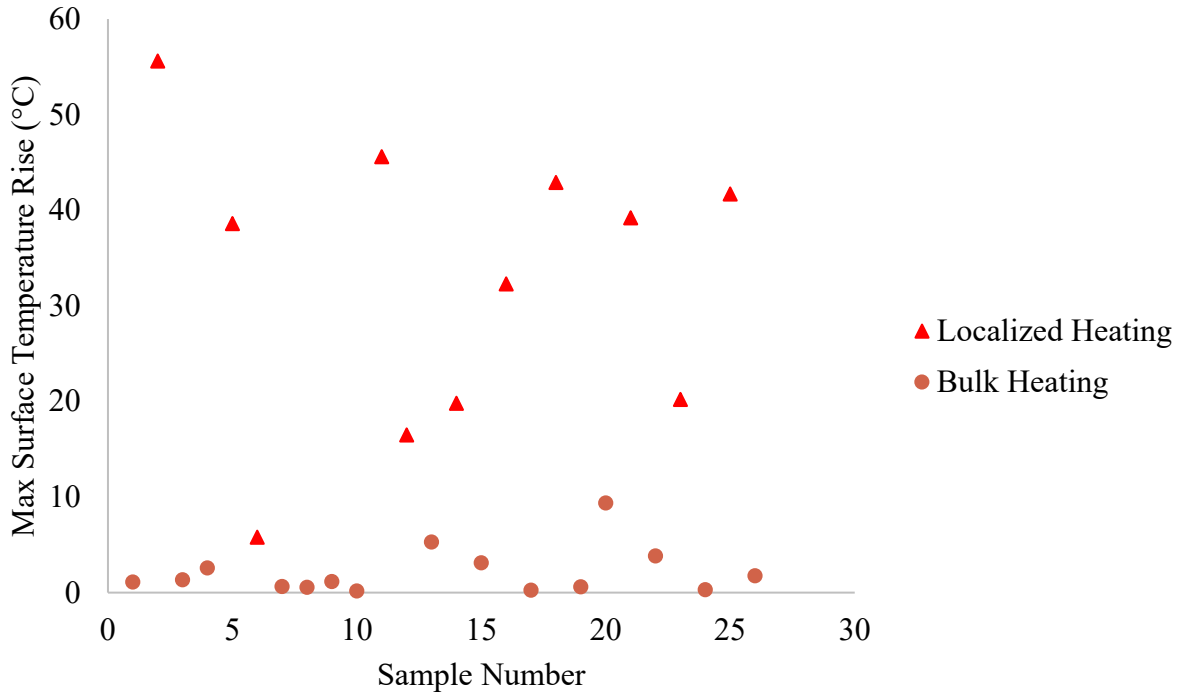


Figure 5.3:Maximum surface temperature rise due to ultrasonic excitation of Sylgard 184/527

The maximum surface temperature rise for each Sylgard 184 5:1 sample was plotted in **Figure 5.4.** 92% of these samples were observed to have the characteristic circular heating pattern indicative of localized heating. 2 samples or 16% of the samples which had this circular heating pattern underwent a reaction and produced significant quantities of gas. In both cases, the temperature at the top surface surpassed the temperature limits of the IR camera. This reaction rate was not unexpected with a previous author seeing ~20% of samples react under similar circumstances with base Sylgard 184 [12]. While the maximum surface temperature rise of these samples ranged from 6 °C to ~118 °C, the subset of samples which had the heating pattern without reacting ranged from 6 °C to 26 °C. Within this subset of samples, the mean was only 12 °C with a median of 9 °C demonstrating a skew to the right, and a respective standard deviation of 7 °C demonstrated significant variation in the heating response. With a median maximum temperature rise only a quarter of the median of the Sylgard 184/527 samples, the Sylgard 184 15:1 samples generally experienced a much lesser degree of heating.

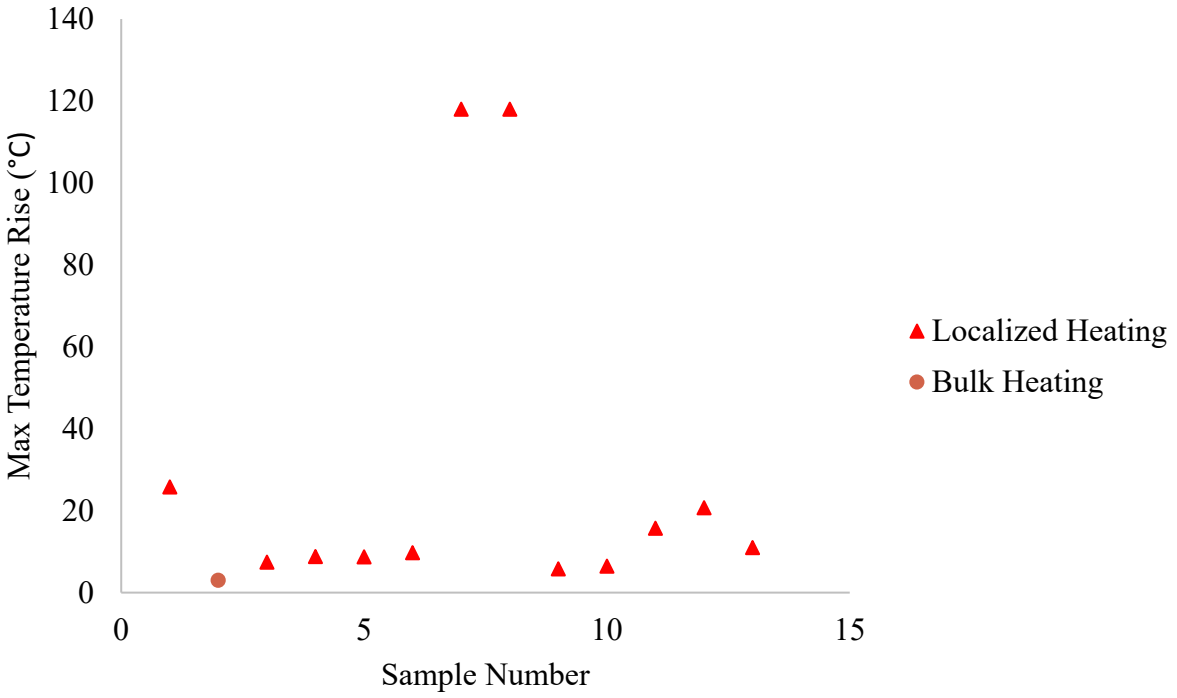


Figure 5.4: Maximum surface temperature rise due to ultrasonic excitation of Sylgard 15:1

Based on these closer examinations of the maximum surface temperature rise data, there are several clear differences. The work of adhesion of these two types of materials was practically identical across all samples, while the elastic modulus varied over approximately an order of magnitude. The softest material, Sylgard 527, showed occasional localized heating with most samples heating to a similar range of temperatures between 30 °C and 60 °C. These Sylgard 527 samples did not undergo a reaction or produce significant amount of gas. Localized heating for the stiffer Sylgard 15:1 material is a very frequent, almost ubiquitous event, but the degree of heating was significantly decreased with most samples achieving a maximum temperature below 30 °C. Two significant exceptions to this behavior occurred when the crystal inclusion was driven to reaction and gas production. This reaction was immediately obvious optically and the temperature increase at the top surface was far in excess of any other non-reacting samples.

Considering the stiffest Sylgard 5:1 material did not exhibit the characteristic circular heating pattern for any samples, it would be reasonable to conclude that a sufficiently stiff material may prevent the thermomechanical mechanism responsible for rapid localized heating from occurring under these excitation conditions. At a threshold of elastic modulus, this particular

dissipation mechanism changes, leading to reaction and gas production. However, this reaction remained relatively rare, and the general maximum surface temperature rise remained relatively low. Further, while the Sylgard 184/527 polymer binder was even more compliant, no reactions occurred even while the average maximum surface temperature rise increased. There may be a complicated relationship over this narrow range of stiffness where the probability of localized heating increases, but the thermomechanical mechanism responsible for driving samples to reaction has become limited by the decrease in elastic modulus.

Returning to comparing these results to the high work of adhesion and low elastic modulus HTPB case, a sufficiently high adhesion may disrupt the thermomechanical mechanism responsible for the observed change in behavior. This may be due to the high adhesion preventing delamination from occurring in the first place, and so the frictional mechanism which relies on relative movement cannot occur. This remains true even though the elastic modulus was in the range where some kind of heating would be expected based on the Sylgard results. The significant difference in these heating results suggested that while the conclusions presented here are likely limited to these particular ultrasonic excitation conditions, there is compelling evidence that both adhesion and stiffness can play a role in the thermomechanical mechanism responsible for localized heating of composite energetic materials under ultrasonic excitation.

## 5.5 Conclusion

This work utilized a single inclusion-binder system to investigate the heating response of compound explosives to strongly coupled ultrasonic excitation. These experiments were carried out with HMX inclusions in cured Sylgard or HTPB matrices. Based on the collected data and the application of previous theories on adhesion, it was evident that there was a significant influence of elastic modulus and the work of adhesion on the degree of localized heating. There was evidence of a complicated relationship between elastic modulus and the degree of localized heating wherein a high elastic modulus prevents heating, but a lower elastic modulus promotes localized heating. However, the heating mechanism responsible for generating sufficient energy to drive the HMX crystal to reaction and gas production appears to be highly sensitive to elastic modulus. A material with a very low elastic modulus appears to somehow limit this mechanism and prevent reaction and gas production from occurring. However, there is significant work remaining to explore this parameter space in order to make definitive generalizable conclusions about practical design

considerations. The conclusions presented here are the product of a simplified single crystal sample under specific excitation conditions, but significant evidence was found that justifies further exploration of the relationship between work of adhesion, elastic modulus, and localized heating.

# 6. FINAL CONCLUSIONS

The objective of this work has been to explore the role of adhesion in the formation of hot spots within composite energetic materials. Ultrasonic excitation and drop weight impact were chosen as two distinct excitation sources in order to explore this space of interest. The work of adhesion and elastic modulus were significantly varied in order to screen for a possible influence of these properties.

The drop weight impact experiments initially revealed that the work of adhesion did not have a significant impact on the drop weight energy of the various PBXs. The largest increases in drop energy, or decreases in sensitivity, occurred as the elastic modulus of the polymer decreased. As the elastic modulus increased, it seemed to have a diminishing impact on the sensitivity. This may have suggested that the mechanism primarily driving the sensitivity behavior of the material changed as the elastic modulus increased. It was posited that the binder acted as a kind of cushion for the energetic crystals, and the lower modulus allowed for this cushioning effect have the maximum impact on the sensitivity behavior. While the effect of the work of adhesion initially seemed to be convoluted with the effect of the elastic modulus, closer examination revealed an independence of the drop energy from the work of adhesion. It is likely that any role of the work of adhesion was minimized in this scenario where the material was compressed. This study highlighted the importance of exploring this lower range of material properties, but further study focused on the small range where the mechanistic transition seems to occur could prove insightful.

The weakly coupled ultrasonic excitation experiments demonstrated a relative independence of the degree of localized heating from the work of adhesion once delamination had occurred. This outcome was well explained by the relatively short range of the adhesion forces. Once the polymer had been delaminated from the crystal surface, close intermolecular contact is not able to be reestablished and adhesion forces are greatly reduced in magnitude. The thermomechanical mechanism responsible for the change of vibrational energy to thermal energy also seemed to be relatively independent of the elastic modulus. In all cases, the loss of intimate molecular contact led to the localization of energy at the interface between the polymer and the crystal. However, the scope of this experiment was relatively narrow, and there remains a large amount of work exploring this kind of excitation.

The strongly coupled ultrasonic excitation experiments demonstrated a strong dependence of the degree of localized heating on the work of adhesion and elastic modulus. The role of adhesion seemed to be to prevent delamination from occurring and a high work of adhesion seemed to prevent the localization of energy as the sample was ultrasonically excited. The elastic modulus seemed to have a more complicated relationship wherein a high elastic modulus prevented the localization of energy, but a sufficiently low modulus prevented enough energy from deposited to drive the sample to reaction. The lower elastic modulus may have allowed for a greater viscoelastic contribution, but sufficient energy for decomposition could not be reached without a minimum elastic modulus. While these observations point to potentially important design considerations for energetic materials, the impact of this project is limited to these particular excitation parameters.

Ultimately, this work revealed important information on the role of adhesion in these PBX systems. While the experiments had a specific scope and purpose, the results of this work can provide insight into the design of new composite energetic materials. In particular, the impact experiments suggest dramatic changes in impact sensitivity can be achieved by decreasing the elastic modulus of the polymer binder. There is also significant evidence that there is more work to be performed either exploring the extremes of these material properties or investigating the role of adhesion in the sensitivity of composite energetic materials to various types of excitation. A comprehensive approach to the design of novel composite energetic materials will require a more complete understanding of how each of these properties influences the specific sensitivity response of the bulk material.

# WORKS CITED


1. Field, J.E., *Hot spot ignition mechanisms for explosives.* Accounts of Chemical Research, 1992. **25**(11): p. 489-496.
2. Bowden, F.P. and A.D. Yoffee, *Initiation and Growth of Explosives*. 1952: Cambridge University Press.
3. Bowden, F.P. and A.D. Yoffee, *Fast Reactions in Solids.* Physics Today, 1959.
4. Loginov, N.P., *Vibration sensitivity of solid explosives.* Combustion, Explosion and Shock Waves, 1995. **31**(1): p. 94-99.
5. Loginov, N., *Structural and physicochemical changes in RDX under vibration.* Combustion, Explosion and Shock Waves, 1997. **33**(5): p. 598-604.
6. Loginov, N., S. Muratov, and N. Nazarov, *Initiation of explosion and kinetics of explosive decomposition under vibration.* Combustion, Explosion and Shock Waves, 1976. **12**(3): p. 367-370.
7. Miller, J.K., D.C. Woods, and J.F. Rhoads, *Thermal and mechanical response of particulate composite plates under inertial excitation.* Journal of Applied Physics, 2014. **116**(24): p. 244904.
8. Mares, J.O., et al., *Heat generation in an elastic binder system with embedded discrete energetic particles due to high-frequency, periodic mechanical excitation.* Journal of Applied Physics, 2014. **116**(20): p. 204902.
9. Mares, J.O., et al., *Localized Heating Near a Rigid Spherical Inclusion in a Viscoelastic Binder Material Under Compressional Plane Wave Excitation.* Journal of Applied Mechanics, 2017. **84**(4): p. 041001.
10. Woods, D.C., J.K. Miller, and J.F. Rhoads, *On the Thermomechanical Response of HTPB-Based Composite Beams Under Near-Resonant Excitation.* Journal of Vibration and Acoustics, 2015. **137**(5): p. 054502.
11. Mares, J.O., et al., *In-situ X-ray observations of ultrasound-induced explosive decomposition.* Applied Materials Today, 2019. **15**: p. 286-294.
12. Roberts, Z.A., et al., *Mesoscale observations of the thermal decomposition of energetic composites under ultrasonic excitation.* Journal of Applied Physics, 2019. **125**(21): p. 215114.

13. Chen, M.-W., et al., *Hot spots in energetic materials generated by infrared and ultrasound, detected by thermal imaging microscopy.* Review of Scientific Instruments, 2014. **85**(2): p. 023705.
14. Mares, J.O., et al., *Thermal and mechanical response of PBX 9501 under contact excitation.* Journal of Applied Physics, 2013. **113**(8): p. 084904.
15. Miller, J.K., et al., *The impact of crystal morphology on the thermal responses of ultrasonically-excited energetic materials.* Journal of Applied Physics, 2016. **119**(2): p. 024903.
16. You, S., et al., *Ultrasonic hammer produces hot spots in solids.* Nature Communications, 2015. **6**: p. 6581.
17. Men, Z., K.S. Suslick, and D.D. Dlott, *Thermal Explosions of Polymer-Bonded Explosives with High Time and Space Resolution.* The Journal of Physical Chemistry C, 2018. **122**(26): p. 14289-14295.
18. Roberts, Z.A., et al., *The effects of crystal proximity and crystal-binder adhesion on the thermal responses of ultrasonically-excited composite energetic materials.* Journal of Applied Physics, 2017. **122**(24): p. 244901.
19. Yeager, J.D., et al., *Nanoindentation of explosive polymer composites to simulate deformation and failure.* Materials Science and Technology, 2012. **28**(9-10): p. 1147-1155.
20. Ahmed, E., M.M. Mohamed, and W. Tamer, *Sensitivity and Detonation Characteristics of Selected Nitramines Bonded by Sylgard Binder.* Propellants, Explosives, Pyrotechnics, 2016. **41**(6): p. 1044-1049.
21. Suceska, M., *Test Methods For Explosives*. 1995, New York: Springer-Verlag.
22. Will, W., Gesamte Schiess. Sprengstoffwesen, 1906(1): p. 209.
23. Kast, H., Gesamte Schiess. Sprengstoffwesen, 1909. **4**: p. 263.
24. Baker, P.J., A.M. Mellor, and C.S. Coffey, *Critical impact initiation energies for three HTPB propellants.* Journal of Propulsion and Power, 1992. **8**(3): p. 578-585.
25. Coffey, C.S. and V.F. De Vost, *Impact Testing of Explosives and Propellants.* Propellants, Explosives, Pyrotechnics, 1995. **20**(3): p. 105-115.
26. Doherty, R.M. and D.S. Watt, *Relationship Between RDX Properties and Sensitivity.* Propellants, Explosives, Pyrotechnics, 2008. **33**(1): p. 4-13.

27. Kamlet, M.J. and H.G. Adolph, *The relationship of Impact Sensitivity with Structure of Organic High Explosives. II. Polynitroaromatic explosives.* Propellants, Explosives, Pyrotechnics, 1979. **4**(2): p. 30-34.
28. Politzer, P. and J.S. Murray, *Impact sensitivity and crystal lattice compressibility/free space.* Journal of Molecular Modeling, 2014. **20**(5): p. 2223.
29. Bondarchuk, S.V., *A unified model of impact sensitivity of metal azides.* New Journal of Chemistry, 2019. **43**(3): p. 1459-1468.
30. Bondarchuk, S.V., *Impact sensitivity of aryl diazonium chlorides: Limitations of molecular and solid-state approach.* Journal of Molecular Graphics and Modelling, 2019. **89**: p. 114-121.
31. Bondarchuk, S.V., *Quantification of Impact Sensitivity Based on Solid-State Derived Criteria.* The Journal of Physical Chemistry A, 2018. **122**(24): p. 5455-5463.
32. Walley, S.M., et al., *The Use of Glass Anvils in Drop-Weight Studies of Energetic Materials.* Propellants, Explosives, Pyrotechnics, 2015. **40**(3): p. 351-365.
33. Swallowe, G.M. and J. E. Field, *The Ignition of a Thin Layer of Explosive by Impact; the Effect of Polymer Particles*. Vol. 379. 1982. 389-408.
34. Field, J.E., et al., *Dynamic Deformation Properties of Energetic Composite Materials*. 2005: Cambridge Univ (United Kingdom).
35. Schedlbauer, F.a.K., A. *The Influence of Particle Size and the Mechanical Properties on the Sensitivity of High Explosive Charges (PBX)*. in *10th Int. Detonation Symposium*. 1995.
36. Manner, V.W., et al., *In Situ Imaging during Compression of Plastic Bonded Explosives for Damage Modeling.* Materials (Basel, Switzerland), 2017. **10**(6): p. 638.
37. EC Martin, R.Y., *Effects of Surface Interactions and Mechancial Properties of PBXs (Plastic Bonded Explosives) on Explosive Sensitivity*. 1984: Naval Weapons Center, China Lake CA.
38. Nicholson, D.W., *On the Detachment of a Rigid Inclusion from an Elastic Matrix.* The Journal of Adhesion, 1979. **10**(3): p. 255-260.
39. Yee, R.Y., and E. C. Martin, *Effects of Surface Interactions and Mechancial Properties of Plastic Bonded Explosives on Explosive Sensitivity. Part 2. Model Formulation*. 1985: Naval Weapons Center China Lake CA.

40. Khanafer, K., et al., *Effects of strain rate, mixing ratio, and stress–strain definition on the mechanical behavior of the polydimethylsiloxane (PDMS) material as related to its biological applications.* Biomedical Microdevices, 2008. **11**(503): p. 8.
41. Hamshere, B.L., Lochert, Ian J., Dexter, Richard M., *Evaluation of PBXN-109: the Explosive Fill for the Penguin Anti-Ship Missile Warhead*, A.G.D.o. Defense, Editor. 2003, DSTO Systems Sciences Laboratory: Edinburgh.
42. Wingborg, N., *Increasing the tensile strength of HTPB with different isocyanates and chain extenders.* Polymer Testing, 2002. **21**(3): p. 283-287.
43. Palmer, S., D. Williamson, and W. Proud, *Adhesion studies between HMX and EDC37 binder system.* AIP Conference Proceedings, 2006. **845**.
44. Rae, P.J., et al., *Quasi–static studies of the deformation and failure of β–HMX based polymer bonded explosives.* Proceedings of the Royal Society of London. Series A: Mathematical, Physical and Engineering Sciences, 2002. **458**(2019): p. 743-762.
45. Bellerby, J.M. and C. Kiriratnikom, *Explosive-Binder Adhesion and Dewetting in nitramine-filled energetic materials.* Propellants, Explosives, Pyrotechnics, 1989. **14**(2): p. 82-85.
46. Yeager, J.D., et al., *Adhesive properties of some fluoropolymer binders with the insensitive explosive 1,3,5-triamino-2,4,6-trinitrobenzene (TATB).* Journal of Colloid and Interface Science, 2010. **352**(2): p. 535-541.
47. Fowkes, F.M., *Additivity of intermolecular forces at interfaces. I. Determination of the contribution to surface and interfacial tensions of dispersion forces in various liquids.* The Journal of Physical Chemistry, 1963. **67**(12): p. 2538-2541.
48. Young, T., *An essay on the cohesion of fluids.* Philosophical Transactions of the Royal Society of London, 1805. **95**: p. 65-87.
49. Nguyen, T. and W.E. Johns, *The effects of aging and extraction on the surface free energy of Douglas fir and redwood.* Wood Science and Technology, 1979. **13**(1): p. 29-40.
50. Owens, D.K. and R.C. Wendt, *Estimation of the surface free energy of polymers.* Journal of Applied Polymer Science, 1969. **13**(8): p. 1741-1747.
51. Kloubek, J., *Development of methods for surface free energy determination using contact angles of liquids on solids.* Advances in Colloid and Interface Science, 1992. **38**: p. 99-142.

52. Kwok, D.Y. and A.W. Neumann, *Contact angle measurement and contact angle interpretation.* Advances in Colloid and Interface Science, 1999. **81**(3): p. 167-249.
53. Roberts, Z.A., et al. *Phase Changes in Embedded HMX in Response to Periodic Mechanical Excitation*. 2017. Cham: Springer International Publishing.
54. Dixon, W.J. and A.M. Mood, *A Method for Obtaining and Analyzing Sensitivity Data.* Journal of the American Statistical Association, 1948. **43**(241): p. 109-126.
55. Langlie, H.J. *A Reliability Test Method for "One-Shot" Items*. 1963.
56. Neyer, B.T., *A D-Optimality-Based Sensitivity Test.* Technometrics, 1994. **36**(1): p. 61-70.
57. Wickham, J.A., S.P. Beaudoin, and S.F. Son, *The role of adhesion and binder stiffness in the impact sensitivity of cast composite energetic materials.* Journal of Applied Physics, 2020. **128**(21): p. 214902.
58. Cawkwell, M.J. and V.W. Manner, *Ranking the Drop-Weight Impact Sensitivity of Common Explosives Using Arrhenius Chemical Rates Computed from Quantum Molecular Dynamics Simulations.* The Journal of Physical Chemistry A, 2020. **124**(1): p. 74-81.
59. Murray, J.S., M.C. Concha, and P. Politzer, *Links between surface electrostatic potentials of energetic molecules, impact sensitivities and C–NO2/N–NO2 bond dissociation energies.* Molecular Physics, 2009. **107**(1): p. 89-97.
60. Zeman, S. and M. Jungová, *Sensitivity and performance of energetic materials.* Propellants, Explosives, Pyrotechnics, 2016. **41**(3): p. 426-451.
61. Preston, D., et al., *Small-scale explosives sensitivity saftey testing: A departure from Bruceton.* AIP Conference Proceedings, 2012. **1426**(1): p. 713-716.
62. Anthony, L., *The Cambridge Dictionary of Statistics.* Reference Reviews, 2003.
63. Palchesko, R.N., et al., *Development of polydimethylsiloxane substrates with tunable elastic modulus to study cell mechanobiology in muscle and nerve.* PloS one, 2012. **7**(12): p. e51499.
64. Leite, F.L., et al., *Theoretical models for surface forces and adhesion and their measurement using atomic force microscopy.* International journal of molecular sciences, 2012. **13**(10): p. 12773-12856.
65. Israelachvili, J.N., *Intermolecular and surface forces*. 2011: Academic press.

66. Ramos, S., et al., *Wetting on nanorough surfaces.* Physical Review E, 2003. **67**(3): p. 031604.
67. Miller, J., et al., *Effect of roughness as determined by atomic force microscopy on the wetting properties of PTFE thin films.* Polymer Engineering & Science, 1996. **36**(14): p. 1849-1855.
68. Fuller, K. and D. Tabor, *The effect of surface roughness on the adhesion of elastic solids.* Proceedings of the Royal Society of London. A. Mathematical and Physical Sciences, 1975. **345**(1642): p. 327-342.
69. Persson, B.N., et al., *On the nature of surface roughness with application to contact mechanics, sealing, rubber friction and adhesion.* Journal of Physics: Condensed Matter, 2004. **17**(1): p. R1-R62.
70. Villar, L.D., et al., *Thermal aging of HTPB/IPDI-based polyurethane as a function of NCO/OH ratio.* Materials Research, 2011. **14**: p. 372-375.

# APPENDIX A: SUPPLEMENTARY GUIDE TO SELECT METHODS

The purpose of this appendix is to supply supplementary info for the purposes of recreating these experiments and accessing data.

## A.1 Work of Adhesion: Contact Angle Measurement

The adhesion at the interface between the energetic inclusion and the polymer binder can be characterized using the thermodynamic work of adhesion which describes the increase in free energy from creating two surfaces. This approach accounts for the fundamental intermolecular forces responsible for adhesion and provides a route for discriminating between weak and strong adhesion. The thermodynamic work of adhesion can be calculated from the surface energies of each component in a system of contacting materials. These surface energies can be determined from simple contact angle experiments as the angle formed between the liquid, solid, and vapor phases was empirically indicative of the involved intermolecular forces. In work by Yeager *et al.* a contact angle measurement method was used to evaluate the adhesive properties of a number of fluoropolymers with potential applications as explosive binders [46]. The general process was outlined below including important equations.

First, the work of adhesion can be written as below where the subscripts on each interfacial surface energy represents a solid-vapor, liquid-vapor, or solid-liquid interaction [47].

$$W_a = \gamma_{SV} + \gamma_{LV} - \gamma_{SL} \tag{2.4}$$

An explicit relationship between the angle formed and the interfacial surface energy components can be found in Young's equation for the equilibrium of a droplet [48].

$$\gamma_{LV} \cos\theta = \gamma_{SV} - \gamma_{SL} \tag{2.5}$$

In order to avoid underestimating the true surface energy, the surface energies must be split into polar and dispersive components which are denoted with the superscripts *p* and *d* respectively [49].

$$\gamma_{SL} = \gamma_{SL}^{p} + \gamma_{SL}^{d} \tag{2.6}$$

Further, the interfacial surface energies can be represented as a geometric mean of the interacting surface energies [50].

$$\gamma_{12} = \gamma_1 + \gamma_2 - 2\sqrt{{\gamma_1}^d {\gamma_2}^d} - 2\sqrt{{\gamma_1}^p {\gamma_2}^p} \tag{2.7}$$

This can be substituted into a final modified Young's equation given below [50].

$$\frac{\cos(\theta)+1}{2} * \frac{\gamma_{lv}}{\sqrt{\gamma_l{}^d}} = \sqrt{\gamma_s{}^p}\left(\frac{\sqrt{\gamma_l{}^p}}{\sqrt{\gamma_l{}^d}}\right) + \sqrt{\gamma_s{}^d} \quad (2.8)$$

Polar and dispersive components of the liquids can be obtained from literature, allowing for determination of the polar and dispersive components of an unknown solid via a simple linear regression [50-52]. An example of this process is shown in **Figure 2.1** and **Figure 2.2** where a drop of a liquid is placed upon a substrate and the angle measured is a product of the various surface energy interactions at the interface.

Figure 2.1: A drop of liquid on a solid substrate

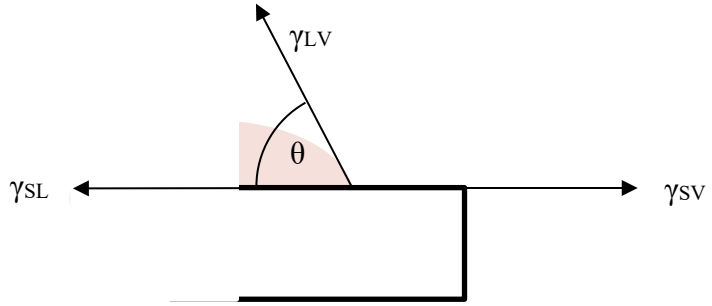


Figure 2.2: Contact angle at the edge of the interface between the liquid drop and the solid substrate where the angle formed is due to a balance of interfacial surface energies

The works of adhesion for the polymer binders were calculated by first evaluating the surface energies of the respective components using advancing stable contact angle experiments wherein water and ethylene glycol were utilized as the liquid phase atop the Sylgard 184 or HTPB solid phases. For each liquid, 6 drops of 1.5 mL were placed upon the cured polymer surface and the contact angles for each drop were measured 3 times for a total of 18 measurements per solid-liquid pairing. A Ramé-Hart advanced goniometer model 500-00 and corresponding angle measurement software, DROPimage Advanced 2.8.03, were used to measure the contact angle formed between the liquid drop and solid surface. The explicit procedure for this is detailed below using equipment from Dr. Stephen Beaudoin's research group.

1. Samples of the solid material of interest were cured in an appropriate mold. PTFE molds allowed for easy removal of the material from the mold. The initial cast of the material yielded a flat disk of material approximately 7.5 cm in diameter and 1 cm in thickness. This was then cut into several rectangular strips 1 cm x 5 cm for ease of testing. In order to ensure that the top surface is a smooth surface, which is necessary for accurate testing, the sample was cured with the top surface open to the air rather than encapsulated in the mold.
2. The sample was placed upon the adjustable specimen stage and a fresh dispenser tip was placed upon the dispenser. The dispenser was aligned such that it was directly over the sample surface. The halogen light source was turned on and brightness was adjusted to a desirable level. The camera was then manually focused on the tip of the dispenser and the platform height was adjusted in order to allow a drop to form and then fall onto the sample surface.
3. The automated dispensing system was turned on and initialized using the DROPimage Advanced 2.8.03 software. In order to avoid contamination of the automated dispenser tube, only DI water was allowed to be utilized to charge the tube and dispenser. Bubbles trapped in the tubes are eliminated by cycling the dispenser until the lines are clear. For contact angle measurements with water, the system was now ready for normal operation. For contact angle measurements with any other liquid, only the dispenser tip was filled with the liquid. This was accomplished by placing a new tip on the dispenser, and filling the dispenser from the tip side while the tip was submerged in the liquid of interest. This allowed for the liquid to be drawn up into the syringe while avoiding contamination of the tubes. Excess liquid clinging to the dispenser tip was removed with a wipe, and care was taken to avoid introducing the new liquid into the dispenser tubes.
4. A drop was placed upon the sample surface and final adjustments of the specimen platform were made. Best performance was achieved when the platform was first adjusted to perfectly level and then fine tuned such that the contact between the surface and the drop can be clearly seen. The droplet often cast a shadow and where this shadow met the drop served as a good indicator of the location of the interface. The contact angle program was initialized from the DROPimage software and a snapshot of the image was captured. Following the program guidelines, four lines were placed so the program could measure

the contact angle on both sides of the droplet. Four more pictures were taken and the same procedure was followed. This yields five measurements which were averaged to give the contact angle measurement. The platform or sample was then adjusted such that a new drop could be placed on the surface and the previous drop could no longer be seen through the camera. This process was repeated 6 times and the final list of contact angle measurements was exported to an external drive.

5. The contact angle measurements were averaged and then the surface energy was calculated using linear regression and **Equation 2.8**.

### A.2 Ultrasonic Testing

The ultrasonic testing process was outlined here as well as the steps to extract the relevant data from the infrared video. Sample creation was thoroughly discussed in the main body of this work.

1. The sample was coupled to the transducer with either ultrasonic gel or ethyl cyanoacrylate depending on the goal of the experiment as outlined in this work. Strongly bound samples were allowed to cure for at least 5 minutes. After setting the signal generator to 210.5 kHz and -3 dbm, the transducer leads were attached to the output of the power amplifier.
2. ExamIR software was used in order to control the camera. The IR camera was placed such that it was directly above the sample, and then the camera was focused at the top surface of the sample. After ensuring that the camera was set to record for the appropriate length of time, the camera began to record. Once recording was confirmed to have begun, the power supply and signal amplifier were used to energize the transducer. After the recording has finished, the power supply and signal amplifier were deenergized. If repeated runs were required, the sample was allowed to cool back to within 1 °C of ambient temperature.
3. ExamIR software was also used in order to view the videos and extract the time-temperature data for further analysis. The maximum surface temperature was collected for the entirety of the recording, and the frame of the video at which the transucer received electrical power was recorded. This frame was determined to be the frame at which significant heating of the transducer or the wire leads became visible. This frame was then used in combination from the time-temperature trace data in order to get initial and final temperatures of the sample surface.

### A.3 Drop Weight Testing

The drop weight testing process was outlined here as well as the steps to extract the relevant data from the infrared video. Sample creation and the sensitivity test were thoroughly discussed in the main body of this work. This work was performed on a custom drop height tower located in FLEX labs using the BAM impact sample holders.

1. An initial drop height and estimated range of drop heights were chosen and input into the Neyer Sentest software. The anvil was aligned and the electromagnet was raised to the desired height. Samples were weighed and then placed within the BAM impact sample holders. Before placing the sample on the anvil, the electromagnet was energized and the drop weight impactor was raised. The electromagnet holding the drop weight was then deenergized allowing the drop weight to fall and impact the sample.
2. Each case was determined to be a go or no-go based on if the following phenomena were observed: flash or sparks, odor due to combustion products, noticeable noise generation, evidence of scorch marks on the cylinders, partially burned material within the cylinders, or significant loss of solid material. The response was recorded in the Neyer Sentest software and a new testing height was generated. The procedure was repeated until 10 successive tests yielded a decreasing predicted sigma. This is covered fully in the main body of this work.
3. Care was taken to ensure thorough cleaning of the BAM cylinders after each impact test so that a single cylinder was used for all tests. The results from the sensitivity testing were then recorded and utilized for further data analysis.